

**Engineering Nanointerfaces for Nanocatalysis**

Journal:	<i>Chemical Society Reviews</i>
Manuscript ID:	CS-REV-10-2013-060389.R1
Article Type:	Review Article
Date Submitted by the Author:	24-Feb-2014
Complete List of Authors:	Wang, Xun; Tsinghua University, Zhang, Zhi Cheng; State Key Laboratory of Heavy Oil Processing, China University of Petroleum Xu, Biao; Tsinghua University, Chemistry

ARTICLE

Engineering Nanointerfaces for Nanocatalysis

Cite this: DOI: 10.1039/x0xx00000x

Zhi-cheng Zhang, Biao Xu and Xun Wang*

Received 00th January 2012,
Accepted 00th January 2012

DOI: 10.1039/x0xx00000x

www.rsc.org/

Interface, referred as the boundary between two phases, has been demonstrated to play a critical role in catalysis. Fundamental understanding of interfacial phenomena occurring in catalysis is in favor of rational design of high-performance catalysts. With the thriving of nanoscience, nanointerface also received tremendous attentions in nanocatalysis. In this review, we focus on the recent advances in the delicate design and the fine control of various complex nanomaterials with well-defined interfaces based on the progress in nano-synthetic methodology, including metal-metal oxide, metal-metal, metal-non-oxide and metal in confined spaces. Then the challenging issues in the synthetic control on nanointerface, based on the authors' experiences, are discussed. Finally, the prospects and outlooks for engineering nanointerface for nanocatalysis towards renewable energy are presented.

1 Introduction

Interface, which is generally referred as the boundary between two domains, has been demonstrated to exhibit fundamentally different properties from those of their bulk counterparts.¹⁻³ In the case of catalysis, when optimizing the catalysts to improve the catalytic performance for an idiographic reaction, one usually has to carefully consider the predominant role of interface in binding, transformation and transport of surface species such as electrons, adsorbents, and intermediates between two domains.⁴⁻⁶ So far, to achieve better reaction activity, selectivity, and stability, a great number of research efforts have been devoted to the interfacial effect in catalysis with the aid of advanced spectroscopies, density functional theory (DFT) calculations in model systems, and other surface/interface probes at the molecular/atomic level. However, due to the ill-defined structure and wide size distribution of the different components, it sometimes becomes difficult for researchers to understand better the reaction mechanism, and thus brings some uncertainty and even debate concerning the precise mechanism over the studied catalysts. For example, there have been several reported results from different research groups that remain to be controversial and even partly contradictory, concerning exposed Au-support interface bearing the responsibility for low-temperature CO oxidation.⁷⁻¹¹ In this context, the rational design and

engineering of the phases with well-defined shapes, sizes, and structures is highly desirable. In the past few decades, thanks to the great progresses in modern synthetic chemistry, it is presently feasible to design nanoparticles (NPs) and complex nanomaterials with uniform shapes and sizes, which is really helpful for gaining more deep insights in the catalytic mechanism. For instance, in the case of heterogeneous catalysis, the wide size distribution of noble metals on support as prepared by conventional impregnation method, usually makes it impossible to precisely recognize the interface effect on catalytic reactivity, while developed colloidal synthesis approaches are able to solve this size-control problem, and thus allow us to isolate the catalytic effect of each individual parameter involved in anchored metal catalysts.

Currently, economical and effective alternative catalysts have been generally recognized as the core of various green technologies to meet the renewable energy demands as urgently expected in our society, which provides higher requirements for the production of various kinds of complex nanomaterials. To enhance the catalytic properties and endow the nanomaterials with multifunctionality in terms of specific area such as photocatalysis, electrocatalysis, heterocatalysis, and so on, many types of advanced complex nanomaterials with tunable interfaces have been built up including metal-metal interface, metal-oxide interface, metal-non-oxide interface (e.g. chalcogenide, carbide, nitride, carbon, and coordination polymer, etc.), and other interfaces (e.g., oxide-oxide, oxide-chalcogenide, phosphate-tungstate, etc.). However, it is noteworthy that although more and more isolated reports on the construction of well-defined nanointerfaces with superior properties have emerged in recent years, a comprehensive overview on their synthetic strategies, unique and tailored

Department of Chemistry, Tsinghua University, Beijing, 100084, P. R. China.

E-mail: wangxun@mail.tsinghua.edu.cn; Fax: +8610 62792791;

Tel: +8610 62792791, Prof. X. Wang

properties, and various applications in nanocatalysis has not been well summarized. While concerning the experimental and theoretical research on physical and chemical properties, and function principles of the fabricated interfaces based on traditional methods, one can read some nice review papers in the literatures.^{12, 13} Our understanding here for engineering nanointerfaces for nanocatalysis is from a new viewpoint, referring to the nanomaterial science. The combination of the efforts presented in this review is believed to pave the way to a wide range of catalytic reactions occurring on interfacial sites.

2. Rational design and control of nanointerfaces for enhanced nanocatalysis

2.1 metal and oxide interface

Heterogeneous catalysts, usually consisting of support (typically metal oxides) and supported phases (typically noble metal NPs), have been employed in a variety of important fields involving chemical industry, pollution prevention, and energy technology.¹⁴⁻¹⁸ It is generally accepted that metal oxides can not only serve as a support to disperse metal NPs, but also improve the catalytic properties through the interaction with metal NPs, i.e. so called *strong metal-support interaction* (SMSI).^{19, 20} Such interaction sometimes can become so prominent that the critical role of metal-oxide interface is often highlighted by many experimental and theoretical studies.²¹⁻²⁵ Recently, such a situation of strong interaction has been particularly disclosed in the case of oxide supported noble metal clusters or even single atoms.^{26, 27} Additionally, more complicating matter is that when pre-synthesized metal-metal or metal-oxide heterophases are subsequently deposited on the oxides, more structural factors need to be taken into account involving mixed metal-metal and metal-oxide interfaces. In this sense, the rational design and careful construction of well-defined metal-oxide interface may thus help us to obtain better catalysts for a desired reaction.

Effect of size control and support type on interfacial reactivity

Heterogeneous catalysis is a complex chemical process occurring at nanosize, multicomponent and dynamic solid surfaces. It has been demonstrated that the catalytic activity and selectivity are highly dependent on the shape, size, and surface structure of supported metal NPs as well as oxides.²⁸⁻³¹ Nevertheless, as real working catalysts, heterogeneous catalysts are so complex systems that effect of aforementioned influencing parameters on the overall performance has to be individually investigated. In previous works with respect to surface science and catalysis, the catalytic reaction occurring on interfacial sites has already been revealed and extensively investigated. However, for most heterogeneous catalysts prepared by conventional preparation methods such as impregnation, co-precipitation, and even deposition-

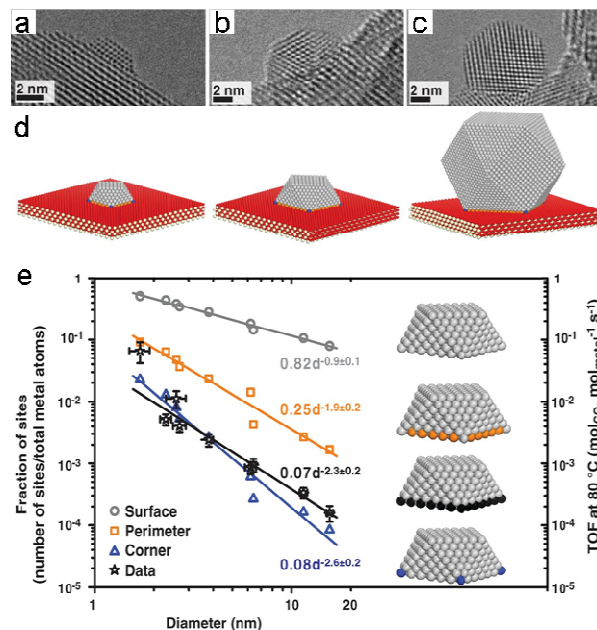


Fig. 1 HRTEM images of Pd/CeO₂ catalysts with different sizes of Pd NPs: (a) small, (b) medium, and (c) large samples. (d) Physical models of metal supported on CeO₂ to show the distribution of surface, perimeter, and corner atoms in contact with the support. (e) Calculated number of sites with a particular geometry (surface and perimeter or corner atoms in contact with the support) as a function of diameter and TOF at 80 °C of the nine ceria-based samples. Adapted with permission from ref. 35. Copyright 2013, American Association for the Advancement of Science.

precipitation, the wide size distribution of metal NPs may prevent us from drawing unambiguous conclusions about metal-oxide interface effect in catalysis. To overcome this problem, the fine size-control of metal NPs to realize monodispersity nature is urgently needed. In recent decades, with the rapid development of modern synthetic methodologies, many strategies have been developed to obtain metal NPs with uniform sizes and shapes on oxide support. This then can simplify the research on interface-involved catalysis and make the researchers understand better the reaction mechanism. In the literatures, the most typical approach to obtain uniform metal NPs is based on wet-chemical synthesis routes, then colloidal deposition method is often adopted to prepare oxide supported metal NPs.³²⁻³⁸ For example, Stucky and co-workers³³ have successfully prepared monodisperse noble metal (Au, Ag, Au–Ag, Pt, Pd) NPs, then deposited these noble metal NPs on different types of oxide supports (Fe₂O₃, TiO₂, ZnO, Al₂O₃, and SiO₂) to unambiguously study the interface effect between noble metal and metal oxide in the selective oxidation of ethanol by oxygen. Very recently, by depositing size-tunable metal NPs on the oxide supports, Murray and co-workers³⁵ found that the length of the CeO₂–metal interfaces could be tailored by the use of monodisperse Ni, Pd, and Pt, in which the relative fraction of interfacial sites was varied for CeO₂ support. In CO oxidation, these CeO₂-based catalysts were demonstrated

to be size-dependent, with a direct participation in the reaction of metal atoms at the perimeter and CeO_2 oxygen lattice. Through colloidal deposition method, many supported catalyst systems have been developed and investigated in order to deeply understand the interface effect in heterogeneous catalysis. Nevertheless, in these synthetic systems, organic capping agents (typically surfactants, polymers, biomolecules) are often used in order to obtain metal NPs with uniform sizes and shapes, which may block the exposure of catalytically active sites. As a consequence, thermal treatments are usually required to remove the capping agent covered on the surface of metal NPs. This process may lead to the agglomeration of metal NPs and thus ultimately complicate the research of interface effect in catalysis. Based on this consideration, the development of effective methods that allow the direct synthesis of metal NPs with clean surface is promising and highly desirable. Recently, Zheng and co-workers³⁹ have presented a surfactant-free strategy to prepare monodisperse Pt NPs from molecular $[\text{Pt}_3(\text{CO})_3(\mu_2\text{-CO})_3]_5^{2-}$ clusters, then deposited as-synthesized Pt NPs on various oxides (TiO_2 , CeO_2 , Fe_2O_3 , and SiO_2). The results show that Fe_2O_3 was the most effective support to make the Pt NPs the most active in CO oxidation, revealing that the interfaces between Pt and Fe_2O_3 are the active sites for O_2 activation in the catalytic reaction. Similar works have also been previously reported in other catalyst systems.^{40, 41}

permission from ref. 45. Copyright 2013, WILEY-VCH Verlag GmbH & Co. KGaA, Weinheim.

Shape, size, and composition control of metal–oxide hybrid nanostructures

The above results reveal that the size of supported metal NPs and the type of oxides can influence the interaction between metal and oxide. Besides, recent researches have shown that the morphologies and surface structures of oxide supports can also affect the loading manner or depositing behavior of metal NPs on them. This further indicates the critical role of interfacial interaction, which can be governed by many influencing factors. For instance, Yang and co-workers⁴² found that by using CeO_2 with different shapes as supports, the growth behavior of Pt could be finely controlled on the CeO_2 via a e-beam evaporation strategy. HRTEM images showed that Pt clusters epitaxially grow on CeO_2 nanooctahedra and randomly grow on CeO_2 nanorods. In CO oxidation reaction, Pt/ CeO_2 nanorods are more active than Pt/ CeO_2 nanooctahedra. In the cyclohexene dehydrogenation, Pt/ CeO_2 nanorods also exhibit a higher activity and selectivity to benzene compared with Pt/ CeO_2 nanooctahedra. Given the importance of morphology-controlled SMSI in the catalytic reactions, as another case, Tsang and co-workers⁴³ demonstrated morphology-dependent interactions of ZnO with Cu NPs at their interface in selective hydrogenation of CO_2 to methanol. They found that the exposed polar (002) facet in ZnO plate exerts a stronger electronic interaction with Cu than other crystal facets, giving a higher methanol yield in CO_2 selective hydrogenation. Very recently, similar work has also been reported in the case of Pd and Ga_2O_3 plate by his group, which makes it more selective for CO_2 activation and hydrogenation.⁴⁴ In addition, Li and co-workers⁴⁵ have reported that, through site-selective growth of noble metals on concave Cu_2O seeds, Pd could solely nucleate on the cavities of concave Cu_2O (Fig. 2a, inset), while Ag mainly grew on edges and vertices of concave Cu_2O (Fig. 2b, inset). This is because the nucleation of metallic components on a substrate usually prefers to occur on highly active sites of defects or surfaces with a large curvature, which has also been demonstrated in other complex systems such as noble metal/semiconductor, metal/oxide, metal/metal, and so on. In the aerobic oxidative arylation of phenylacetylene, the highly improved catalytic activities of these hybrid nanostructures have been investigated relative to the single component counterpart and their physical mixtures (Fig. 2). With the help of XPS spectra and DFT calculation results, they consider that synergistic effect of the hybrid nanostructures in which the electron transfer from the noble metal part to the Cu_2O host may be responsible for the enhancement in catalytic activity.

In contrast to oxide supported metal NPs, metal-oxide heterostructure (typically dumbbell) may provide a convenient way to accurately control the interaction between two dissimilar nanoscale domains, as well as their composition and size at nanoscale tuning capability. This strategy can allow us to isolate the catalytic effect of each individual parameter

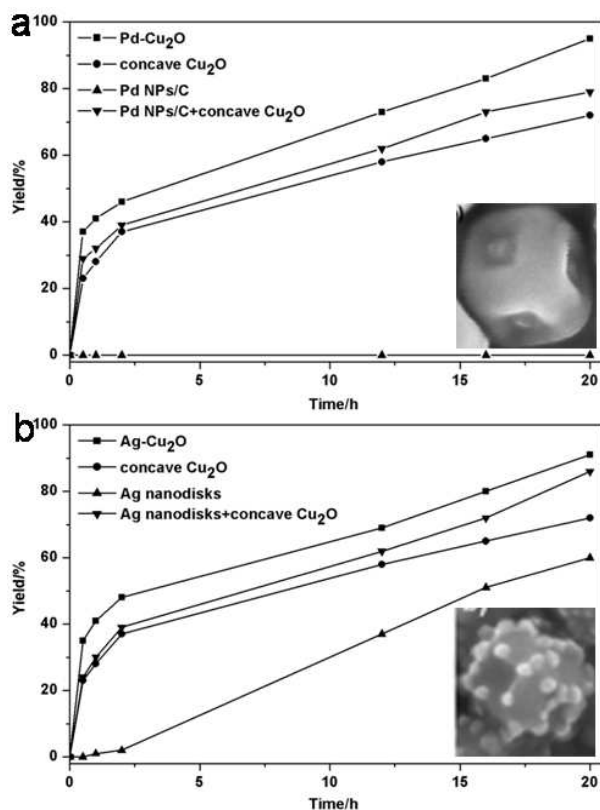


Fig. 2 Catalytic activity of (a) Pd– Cu_2O and (b) Ag– Cu_2O hybrid nanostructures as a function of reaction time in the aerobic oxidative arylation of phenylacetylene. Adapted with

involved in oxide supported metal catalysts. At present, the approaches to construct the heterostructures are mainly based on seed-mediated method. In the case of a dumbbell structure, noble metal NPs are usually preformed as seeds, then oxide epitaxially grows on the surface of metal NPs to form core-shell structures. Upon annealing, the metal nanoparticle is finally partially bound to metal oxide domain. Sun and co-workers⁴⁶ pioneered the synthesis of Au-Fe₃O₄ dumbbell NPs. In their system, the size of the NPs can be tuned from 2 to 8 nm for Au and 4 to 20 nm for Fe₃O₄. After then, the dumbbell nanostructures have been further developed and extensively studied in catalysis, including Au-Fe₃O₄,⁴⁷⁻⁵² Pt-Fe₃O₄,^{48,53} AuAg-Fe₃O₄,⁴⁸ PtPb-Fe₃O₄,⁵⁴ PtPd-Fe₃O₄,⁵⁵ FePt-Fe₃O₄,⁵⁶ Ag-Fe₃O₄,^{48, 57,58} Au(Ag)-MnO₂,⁵⁹ Co-TiO₂,⁶⁰ AuPd-Fe_xO_y.⁶¹ In these catalyst systems, the enhancement in catalytic activities is proposed to arise from the partial charge or electron transfer at the nanoscale interface, either from oxide to metal or from metal to oxide. In heterogeneous catalysis, to further improve the catalytic performance, the dumbbell NPs are usually deposited onto support. In that case, two kinds of interfaces effect in catalysis then have to be considered. It is believed that the interface between metal NPs and oxide inside the dumbbell nanostructure can ensure structural stability and prevent the sintering of metal domains, while the interface between dumbbell NPs and support can be controlled to enhance the catalytic performance (Fig. 3). Therefore, coupling with metal-metal heterostructures, metal-oxide dumbbell nanostructures are emerging as a fascinating class of hybrid nanomaterials to study the interface effect in catalysis and are expected to expand the diversity of nanomaterials and range of potential applications.

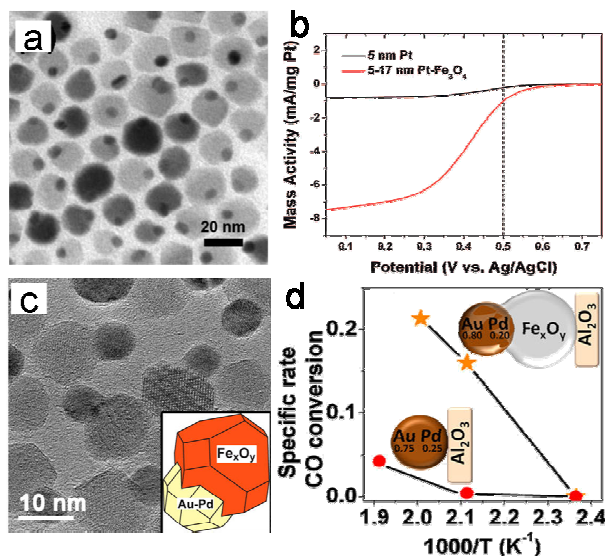


Fig. 3 (a) TEM image of Pt-Fe₃O₄ dumbbell NPs. (b) ORR mass activity for amorphous carbon supported 5 nm Pt and 5-17 nm Pt-Fe₃O₄ dumbbell NPs in 0.5 M H₂SO₄ with the RDE rotation speed at 1600 rpm and sweeping rate at 10 mV/s. (c) TEM image of AuPd-Fe₃O₄ dumbbell NPs. (d) CO oxidation specific rate (mmol converted CO/mmol metal

loading per second) for both AuPd/ and AuPd-Fe_xO_y/Al₂O₃. Adapted with permission from ref. 53. Copyright 2009 American Chemical Society and ref. 61. Copyright 2013, American Chemical Society.

Multiple metal-metal oxide interfaces—a tandem catalyst

In heterogeneous catalysis, a fundamental understanding of relationships between structures and properties of oxide supported metal catalysts is of great importance to identify the catalytically active sites. Whereafter, one can design and construct a sophisticated catalyst for a desired reaction. In this regard, several assembly structures with well-defined shapes have been successfully constructed, during which the multi-interfaces between different domains have been demonstrated to play a crucial role in catalytic process. During past several years, to obtain high-performance, multifunctional nanostructured catalysts for multiple-step chemical reactions, new concepts for the rational design and assembly of multiple metal-metal oxide interfaces referring to a tandem catalyst have been proposed. For example, by the repeated use of the Langmuir-Blodgett (LB) method, a CeO₂-Pt-SiO₂ tandem catalyst has been successfully prepared (Fig. 4). The CeO₂-Pt interface catalyzed methanol decomposition to produce CO and H₂, which were subsequently used for ethylene hydroformylation catalyzed by the nearby Pt-SiO₂ interface. Hence, propanal was produced selectively from methanol and ethylene on the nanocrystal bilayer tandem catalyst.⁶² Similar concepts have also been introduced in other catalyst systems such as TiO₂-Au-SiO₂,^{63, 64} MnO_x-Au-SiO₂,⁶⁵ TiO₂-Au-Fe₃O₄,⁵¹ SiO₂-Pt-TiO₂,⁶⁶ CeO₂-Au-SiO₂.⁶⁷ Inspired by these progresses, we anticipate that the design of multicenter and multifunctional nanostructures to optimize the catalytic performance can also be achieved in multicomponent core-shell structures with multi-shells.

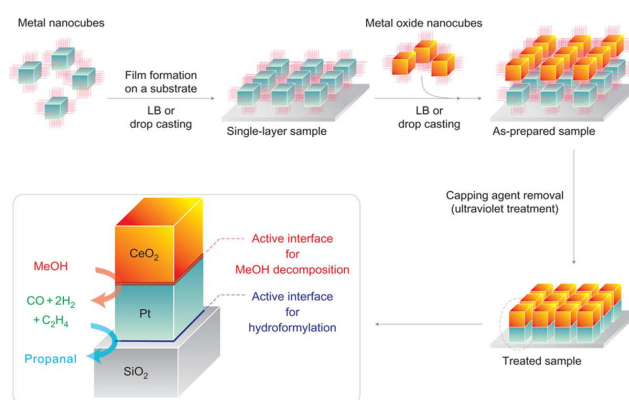


Fig. 4 Assembly process for the preparation of a nanocrystal bilayer 'tandem catalyst'. Adapted with permission from ref. 62. Copyright 2011, Nature Publishing Group.

Oxides confined on metal nanoparticle—an inverse catalyst

Traditional heterogeneous catalysts are usually composed of metal NPs supported on metal oxides. In sharp contrast, recent studies indicate that reducible transition metal oxides covering noble metal surfaces to form the inverse catalysts could remarkably improve the catalytic performance when controlled in a proper way, in which the active oxide phase can be confined by the oxide-metal interface.^{68–72} Taking advantage of this newly developed concept, several groups have design various highly efficient oxide/metal catalysts, including TMO_x/Pt (TM= Fe, Co, and Ni),^{68,69} $\text{Fe}_x\text{O}_y/\text{Rh}$,⁷⁰ $\text{NiO}_{1-x}/\text{Pt}/\text{Ni}$ sandwich structure.⁷¹ It is believed that this strategy will undoubtedly expand great opportunities and stimulate extensive investigations for rational design of oxide/metal catalysts, referring to the concept of nanosynthesis.

2.2 Metal and metal interface

Based on the mixing pattern of two different components, three major types of structures can be formed for bimetallic nanocrystals (NCs): (1) core-shell structure; (2) heterojunction structure; (3) intermetallic or alloyed structures.⁷³ Bimetallic NCs have already been attracting extensive scientific and technological interest because of their superior properties relative to their individual component, and wide use in numerous important fields from science and engineering to technology.^{74, 75} Previous studies have shown that the shape, size, composition, and surface/interface structure of bimetallic NCs can influence their catalytic properties.^{76–84} In this regard, shape-controlled synthesis of bimetallic NCs is highly desired to regulate their performance for various catalytic applications. The two metal components in a bimetallic system can induce synergistic effect, which is often advantageous to the enhancement in catalytic performance due to their unique properties including charge transfer, atomic arrangement, interfacial stabilization, and so on.⁷⁶ In the following, we concentrate our discussions of metal-metal interfacial effect in catalysis on core-shell and heterojunction structures, due to the presence of well-defined interfaces in the two structures.

Metal-metal core-shell structures

According to reported literatures, seed-mediated growth method has been viewed as the most effective route to fabricate core-shell structures, based on which the shape, composition, and size of the core and shell can be intentionally varied to achieve better catalytic properties.^{85–88} For example, Sun and co-workers⁸⁹ have recently reported a seed-mediated growth approach to prepare core-shell FePtM-FePt (M=Pd, Au) nanowires with 2.5 nm FePtM seeds and 0.3–1.3 nm thick FePt shell (Fig. 5a-d). In oxygen reduction reaction (ORR), they found that these FePtM-FePt nanowires exhibit enhanced activity and durability compared with their corresponding alloy, and show shell thickness and core composition-dependent electrocatalytic activity. Moreover, FePtPd-FePt nanowires exhibit a higher activity than FePtAu-FePt nanowires (Fig. 5e, f). They consider that the possible electronic effect of Pd to

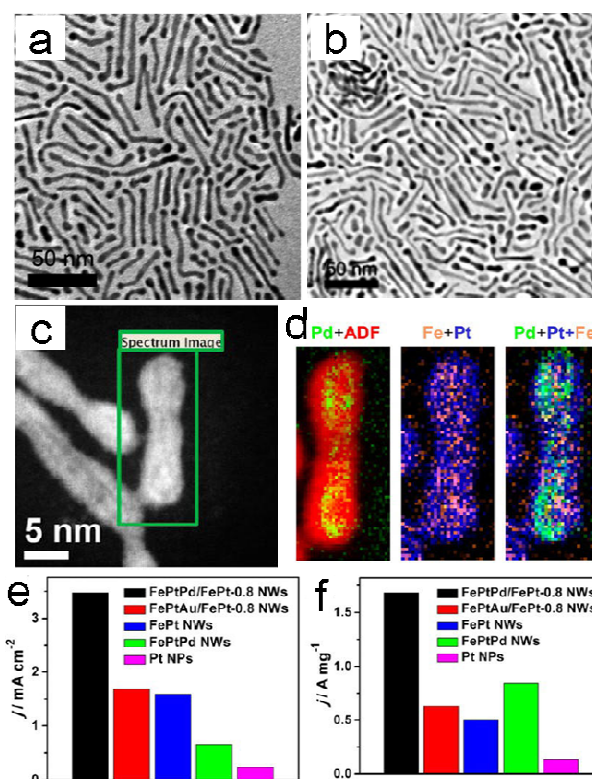


Fig. 5 TEM images of (a) FePtPd-FePt-0.8 and (b) FePtAu-FePt-0.8 . (c) HAADF-STEM and (d) STEM-EELS mapping images of FePtPd-FePt-0.8 . (e) ORR specific and (f) mass activity summaries of the FePtPd-FePt-0.8 , FePtAu-FePt-0.8 , FePt , and FePtPd nanowires as well as the commercial Pt NPs at 0.5 V vs. Ag/AgCl (4 M KCl). Adapted with permission from ref. 89. Copyright 2013, American Chemical Society.

FePt may facilitate O_2 adsorption, activation and desorption. The highest mass and specific activity observed from FePtPd-FePt nanowires with a shell thickness of 0.8 nm may arise from the electronic effect and strain effect. Furthermore, the nanoscale architectural control of the metal-metal interface can be used to tune the geometric and electronic structure of the active sites, while these characteristic properties can determine the d-band center. For instance, as shown in Fig. 6, Tsung et al.⁹⁰ used cubic Pd NPs as seeds to successfully prepare Pd-Rh core-island-shell NPs. Then by using post-synthesis method to control metal migration at the atomic level, Pd-Rh nanoboxes and Rh nanoframeworks can be obtained. In the electrocatalytic evaluation (i.e., CO -stripping, formic acid oxidation, ethanol oxidation, and oxygen reduction reaction), they found that the lattice strain and composition at the surface/interface were the most important factors influencing their catalytic behaviors. More recently, Li and co-workers⁹¹ have developed an effective strategy to achieve the atomic-level design of tri- or multimetallic core-shell structures, referring to the newly developed concept of defect-dominated shape recovery of NCs (Fig. 7). They used concave octahedral Pt_3Ni as seeds, whose

surfaces possess a high density of atomic steps and defects. They then demonstrated that the third metal having the same crystal structures and similar atomic radius with seed can selectively nucleate on the defect sites to achieve the rational design of trimetallic $\text{Pt}_3\text{Ni}@M$ core-shell structures ($M = \text{Au}, \text{Ag}, \text{Cu}, \text{Rh}, \text{Ni}$). In subsequent catalytic reactions, by controlling the depositing behavior and coverage density of the third metal, they confirmed that these multicenter and multifunctional nanostructures could significantly improve catalytic performance due to the geometrical and electronic effects between seed and the third metal. In addition to the seed-mediated growth method, some other encouraging approaches have been recently developed to achieve the sophisticated design of bi- or multimetallic core-shell nanostructures, involving underpotential deposition replacement, electrochemical de-alloying and chemical-reaction-driven reconstruction.⁹² Because of the flexibility in composition and geometric structure, these multimetallic core-shell and even multi-shell complex nanostructures are becoming increasingly appealing and will offer new opportunities for wide scientific communities.

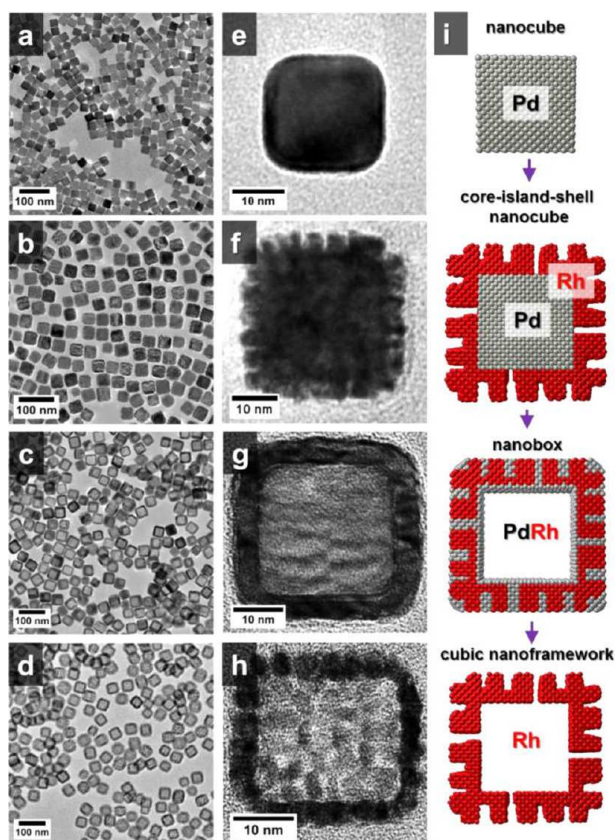


Fig. 6 TEM images of (a, e) Pd nanocubes, (b, f) Pd–Rh core-island-shell nanocubes, (c, g) Pd–Rh nanoboxes, and (d, h) Rh cubic nanoframes. A scheme in (i) shows models for the structural evolution from Pd nanocube to Rh cubic nanoframe. Adapted with permission from ref. 90. Copyright 2013, American Chemical Society.

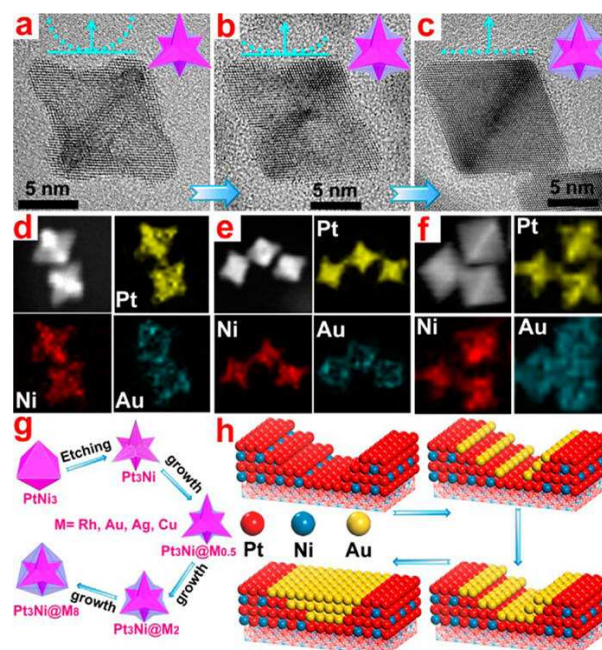


Fig. 7 (a–c) SA-corrected HRTEM images of (a) $\text{Pt}_3\text{Ni}@M_{0.5}$, (b) $\text{Pt}_3\text{Ni}@M_2$, and (c) $\text{Pt}_3\text{Ni}@M_8$. (d–f) Elemental maps of (d) $\text{Pt}_3\text{Ni}@M_{0.5}$, (e) $\text{Pt}_3\text{Ni}@M_2$, and (f) $\text{Pt}_3\text{Ni}@M_8$. (g) Schematic illustration of the evolution from octahedral PtNi_3 to $\text{Pt}_3\text{Ni}@M_8$ ($M = \text{Rh}, \text{Au}, \text{Ag}, \text{Cu}$). (h) Schematic illustration of the growth of Au on the Pt surface. Adapted with permission from ref. 91. Copyright 2013, American Chemical Society.

Metal–metal heterostructures

Compared with metal-metal core-shell structures with only one metal exposed, metal-metal heterojunction structures with both two metals and their interface exposed are more suitable structures to study metal-metal interfacial reactivity, and thus have attracted tremendous research interests.⁷⁶ Up to now, several strategies have been developed to construct metal-metal heterojunction structures: (1) seed-mediated growth approach,^{93–97} (2) galvanic replacement reaction,^{98–100} and (3) successive or simultaneous reduction of metal precursors in one-step synthesis.^{101,102} By using these methods, all kinds of metal-metal heterostructures with different dimensions, sizes, and/or compositions have been designed and adequately demonstrated to show enhanced catalytic or electrocatalytic properties, due to synergistic effects of two metals in charge transfer, interfacial collaboration, or structural strain. Inspired by the promotional effect of metal-metal interface in catalysis, it is pivotal to statistically acquire as many interfaces as possible.^{103, 104} With this aim, Yu and co-workers¹⁰⁴ have recently developed one-step electrodeposition route on an anodic aluminum oxide template to fabricate Pd–Au bimetallic NPs tubes with a tunable interface (Fig. 8). Pd and Au NPs are homogeneously dispersed in the tubes and thus can provide numerous interfaces. Moreover, the interface sites can be qualitatively controlled by tuning the proportion of Pd and Au

NPs. In the electro-oxidation of ethanol, they found that the activity is principally relative to the interface sites and has no direct relation with single metal component in the tube. This significantly enhanced effect of Pd and Au may be ascribed to the electronic structure and local reactivity and a significant coupling of d orbitals at the Pd–Au interfaces.

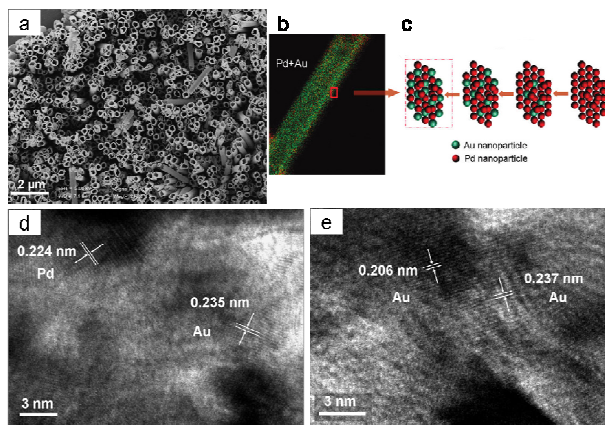


Fig. 8 (a) SEM and (b) EDX mapping images of Pd–Au bimetallic NPs tubes. (c) Simplified schematic illustration of the interface increase with increasing of the Au ratio. HRTEM images of (d) overlapped Pd–Au particles near the edge of the pore area, and (e) Au–Au particle interface, respectively. Adapted with permission from ref. 104. Copyright 2013, American Chemical Society.

2.3 metal and non-oxide interfaces

Metal–carbon interface

Carbon, as another conventionally used support, also received renewed attentions since the thriving of nanoscience. New polymorphs of carbon materials such as 1D carbon nanotube (CNT),¹⁰⁵ 2D graphene,¹⁰⁶ and analogs of graphitic carbon such as C_3N_4 ¹⁰⁷ have all attracted enormous interests. Unlike metal-like conducting graphite counterpart, these new forms of carbon materials exhibit tunable electronic structures, ranging from metal, semi-metal to semiconducting. For example, CNT could be tuned to metal-like or semiconducting through different rolling styles.¹⁰⁵ Single layer graphene is semi metal, while upon layer engineering, doping, or oxidation, the electronic structure could be altered.¹⁰⁶ This provides many possibilities to tune the catalytic performance through support–metal interactions. These carbon-supported noble metal catalysts have been reviewed by a series of excellent papers^{108,109} and the readers can refer to them.

Metal–metal chalcogenides/nitride/carbide interfaces

Apart from the most commonly used carbon and metal oxide support, some other binary compounds (chalcogenides, nitrides, carbides), most of which are semiconductors, can also be

utilized as electronic-active support materials. In terms of nanosynthesis, chalcogenides are the most convenient to tackle with. It is quite difficult to tune the mesostructure of nitrides and carbides through wet chemical routes due to the high energy barrier for formation of the phases. Usually high-temperature solid state route were utilized to prepare a nitride¹¹⁰ or carbide support.¹¹¹ Subsequent deposition of noble metal NPs afforded excellent catalyst, in a wide range of application, as exemplified by electrocatalysts. Recently, colloidal route was established for nitride¹¹² and phosphide¹¹³ NCs, which opened up the possibility for constructing nanointerface between these binary compound and metal. However, in this section, we still mainly concentrate on chalcogenides due to the well-developed synthetic strategies.

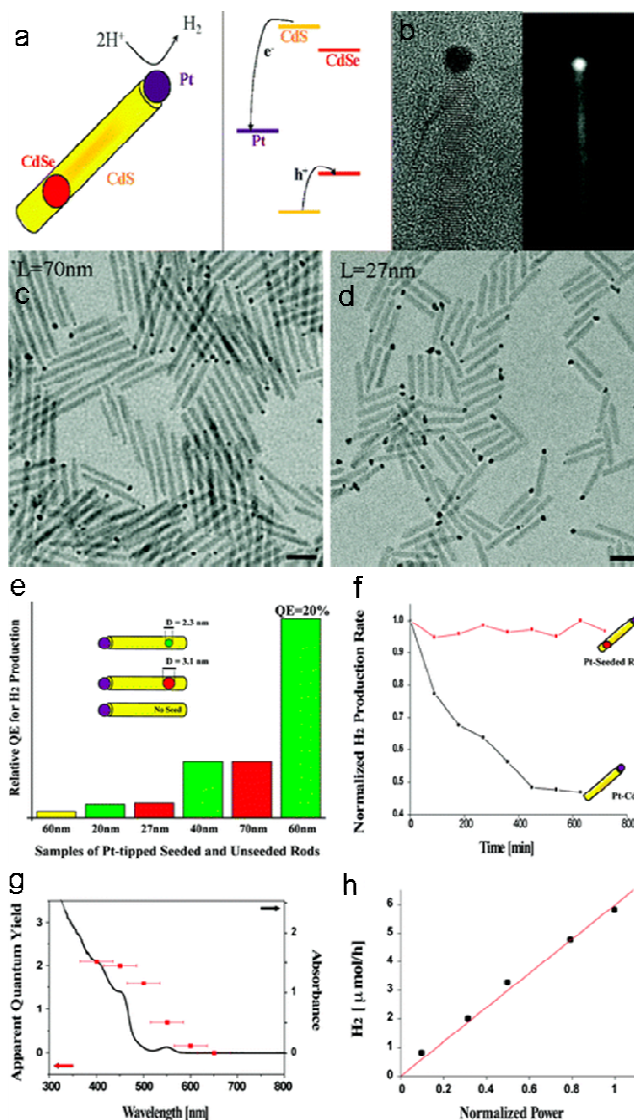


Fig. 9 (a) Schemes on band alignment of CdSe@CdS–Pt nanostructure and (b) corresponding bright-field and dark-field TEM images, (c, d) TEM images of different-length nano-heterostructures (NHSS), (e) Photocatalytic hydrogen evolution performance of different NHSS, (f) time course of hydrogen

evolution of different NHSs, (g) Apparent quantum yield and UV-Vis spectra of the NHSs, (h) rate of hydrogen evolution under different power of illumination. Adapted with permission from ref. 121. Copyright 2010, American Chemical Society.

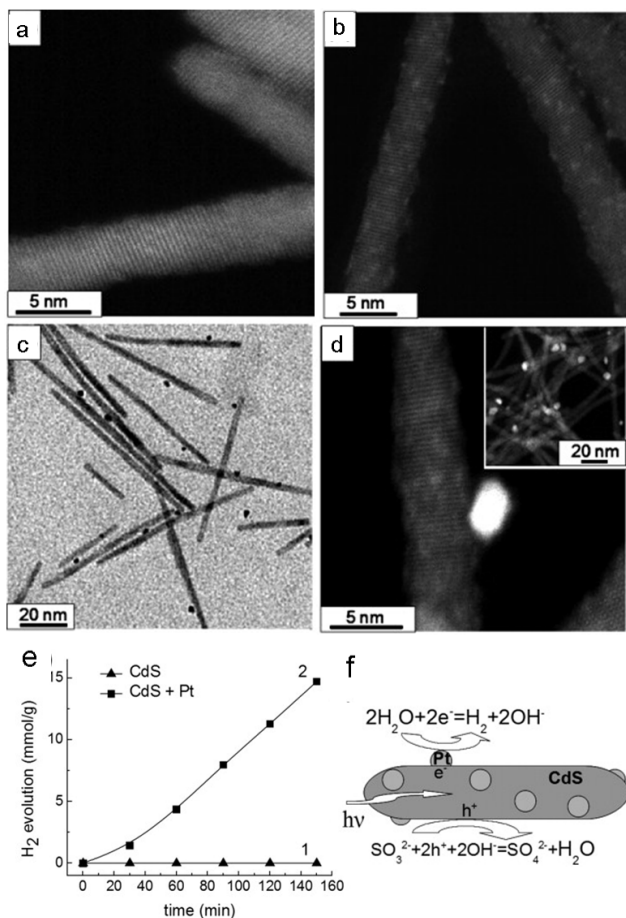


Fig. 10 (a) HAADF-STEM image of non-decorated CdS nanorods, (b) HAADF-STEM image of CdS nanorods decorated with Pt clusters, (c) TEM and (d) HAADF-STEM images of CdS nanorods decorated with both Pt clusters and a Pt nanoparticle. (e) Photocatalytic hydrogen generation (in mmol of H₂ per gram of CdS; more than 99% of incoming light is absorbed by the sample) from an aqueous solution containing CdS nanorods non-decorated (1) and decorated with Pt (2). The curve (2) presents both the samples as shown in b and d (or c). (f) Schematic illustration of the hydrogen generation process. Adapted with permission from ref. 123. Copyright 2010, AIP.

Chalcogenides were usually regarded as poisons in catalysis because sometimes the leached chalcogen species would strongly coordinate with the noble metal atoms and blocked the active sites.¹¹⁴ However, under low-temperature conditions especially in photocatalysis or electrocatalysis, this drawback might be avoided.

In the field of photocatalysis, chalcogenides materials have been widely used for photocatalytic hydrogen evolution.¹¹⁵ To enhance the separation of hole and electron under illumination, noble metals, especially Pt was deposited onto the surface of

the semiconducting chalcogenides.¹¹⁶⁻¹²⁰ The underlying mechanism could also be regarded as the modulation of cold electrons. With the advances in nanosynthesis, the structure of the photocatalysts could be finely tuned as exemplified by the recent work of Alivisatos et al.¹²¹ They prepared CdS nanorods and CdSe NPs @ CdS nanorods core-shell structures (Fig. 9) with precise engineering on the size of CdSe core and aspect ratio of the CdS nanorods. The introduction of CdSe core constructed an inverse Type I band alignment through the CdSe–CdS interface and facilitated the separation of electron and hole. Furthermore, with quantum confinement effect, the size variation also modulated the band structure of the CdSe and hence tuned the band alignment at the CdSe–CdS interface. The performance of these nano structures strongly depended on the radius of CdSe core and the aspect ratio of the nanorods. The deposition of Pt NPs on the tip of CdS nanorod significantly enhanced the activity of photocatalysis. In a subsequent work, Mikhail et al.¹²² etched CdS away in the vicinity of the CdSe core and acquired even better performance. Aside from the modulation of semiconductors, the size control of Pt is also very important and even governs the photocatalytic activity. For example, Rogach and co-workers¹²³ have recently demonstrated that CdS nanorods decorated with subnanometer sized Pt clusters exhibit excellent activity for photocatalytic hydrogen production, as compared to those with large Pt nanoparticles (Fig. 10). The results presented here also indicate substantial reduction of material costs.

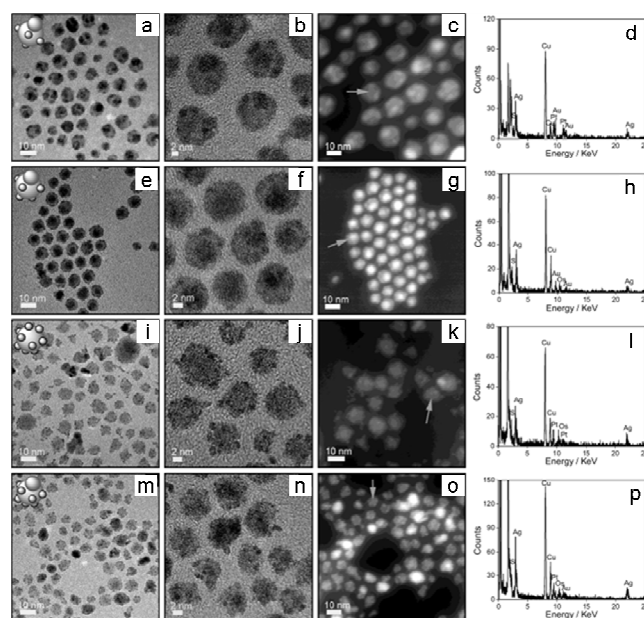


Fig. 11 (a) TEM, (b) HRTEM, and (c) HAADF-STEM images and (d) EDX analysis of Ag₂S–Au–Pt nanocomposites. (e) TEM, (f) HRTEM, and (g) HAADF-STEM images and (h) EDX analysis of Ag₂S–Au–Os nanocomposites. (i) TEM, (j) HRTEM, and (k) HAADF-STEM images and (l) EDX analysis of Ag₂S–Pt–Os nanocomposites. (m) TEM, (n) HRTEM, and (o) HAADF-STEM images and (p) EDX analysis of Ag₂S–Pt–Os nanocomposites.

Ag₂S–Au–Pt–Os nanocomposites. Adapted with permission from ref. 124. Copyright 2011, WILEY-VCH Verlag GmbH & Co. KGaA, Weinheim.

Apart from the improvement of the chalcogenides by noble metal, the chalcogenides could also serve as support to enhance the functionality of the noble metals. Similar to oxide support, electron communication between the chalcogenide and noble metals explained the synergic effects. For instance, Ying et al reported a general synthesis of nano silver sulfide (Ag₂S)-supported noble metal electrocatalysts via a phase-transfer method,¹²⁴ including Ag₂S–Pt, Ag₂S–Au–Pt, Ag₂S–Au–Os, Ag₂S–Pt–Os, Ag₂S–Au–Pt–Os nanocomposites, etc. (Fig. 11). The noble metals were grown on Ag₂S NPs as small islands, as evidenced by TEM, HRTEM, HAADF-STEM and EDX analyses. The oil-water interface was crucial for the control of these nanostructures, through well-regulated mass-transfer and reaction. They carried out XPS investigation on Pt and proposed that electrons flow to Pt and bring about the improvement in performance and stability in CO-stripping and methanol oxidation reaction. Further studies also incorporate these metal-sulfide-based heterostructure into thermal catalysis of a three-component coupling reaction and the interface between metal sulfide (CdS, PbS) and gold also facilitate the activation of alkynes. These sulfide supported noble metal catalyst stand for alternatives toward conventional oxide-supported catalyst in terms of convenient wet-chemical processing and structure-tunability.

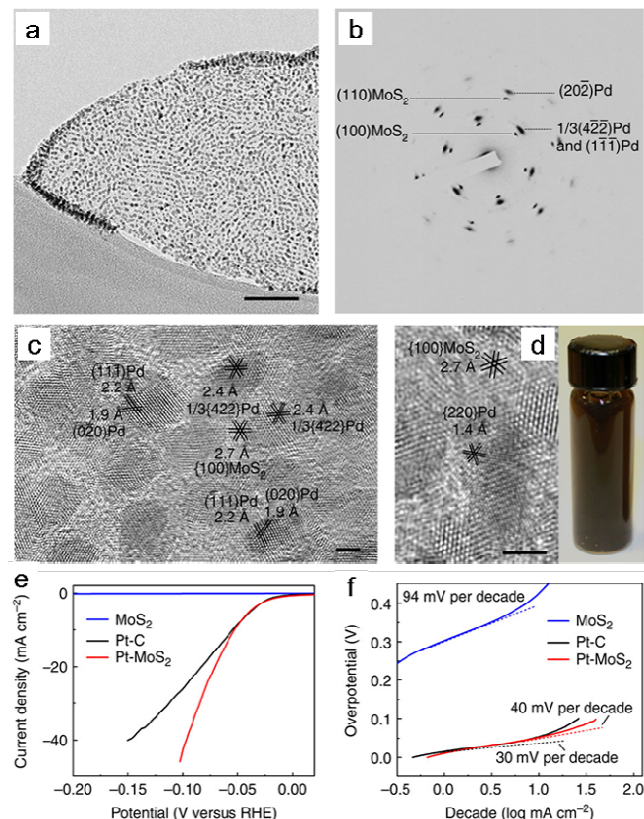


Fig. 12 (a) TEM and (b) SAED pattern of the Pd–single layer MoS₂ heterostructure, (c) corresponding HRTEM images, (d) digital graph of dispersion of Pd–MoS₂ NHSS, (e) i–V scans and (f) Tafel plots of commercial Pt–C, MoS₂ and Pt–MoS₂ electrocatalysts, in 0.5 M H₂SO₄. Adapted with permission from ref. 126. Copyright 2013, Nature Publishing Group.

In addition to traditional chalcogenide NPs, recently, grapheme-like, layered transition metal chalcogenides (such as MoS₂, WS₂) have attracted lots of attentions in electrocatalysis, especially hydrogen evolution reaction (HER).¹²⁵ The tendency to grow in two dimensions also initiates the possibility to tune the sulfide-metal interface through crystal-facet engineering of both parts. Zhang et al realized the epitaxial growth of noble metal NCs (Pd, Ag, Pt) with diameters below 10 nm on a single-layer MoS₂ nanosheet (Fig. 12).¹²⁶ They analyzed the epitaxial orientation and found that the nanostructures show the major (111) and (101) orientations on the MoS₂ (001) surface. The as-obtained Pt–MoS₂ composite exhibited enhanced performance towards the HER reaction when compared with both the single component. XPS was carried out to reveal that there existed electron transfer between Pt and MoS₂. The authors proposed that the defined crystal facets and the selective orientation at the interface would be beneficial for its functionality. However, further control experiments based on systematic control of different exposed facets or crystal axis through the interface are required to verify the assumption.

In the last decades, hot electrons from excitation by photons received emerging attentions due to the clean and sustainable feature of the solar energy.¹²⁷ Metal-semiconductor nano-junctions stand for an efficient platform to utilize hot electrons. In a recent work by Jeong et al.,¹²⁸ single-tipped and double-tipped Pt–CdSe matchstick-like nanoheterostructure were successfully synthesized (Fig. 13). Pump-probe experiments revealed that Platinum NPs efficiently extracted electrons from the CdSe nanorod. Then CO oxidation was tested on this heterostructure and it was found that upon photo excitation, the TOF values increased significantly in a wide range of temperature. As a proof of the concept, if the platinum NPs were grown on an insulating silica substrate, such a photo enhancement in reactivity disappeared. Furthermore, differently doped n-type and p-type GaN substrate was also tested to prove the hot-electron effect in platinum based metal-semiconductor junction.

As a future prospect on metal-chalcogenide nanointerface, we would like to highlight the recent progress in size, composition and shape controlling of the metal nanoparticle in a metal-chalcogenide heterojunction. As known in size-,¹²⁹ composition-¹³⁰ and shape-⁸² tuning in single metal nanoparticle, these factors are proven to be quite crucial for the catalytic performance. However, in a metal-sulfide heterostructure, the fine tuning of these features remains fresh and undeveloped. Yang et al. demonstrated the growth of Pt based alloy NPs, such as PtNi and PtCo on the tip of CdS nanorod (Fig. 14).¹³¹ Ryan et al. reported size-selective growth

of Au NPs on tips of CdSe nanorod (Fig. 14).¹³² Alivisatos et al realized the deposition of Pt nanocube and the exposure of {001} facets of them on a CdS nanorod (Fig. 14).¹³³ However, no further contributions on the property-structure relationships were carried out on these delicate nanostructures. We foresee that with the future thriving in synthesis of size, composition and facet-controlled metal-sulfide nanoheterostructure, the functionalities of them would be exploited.

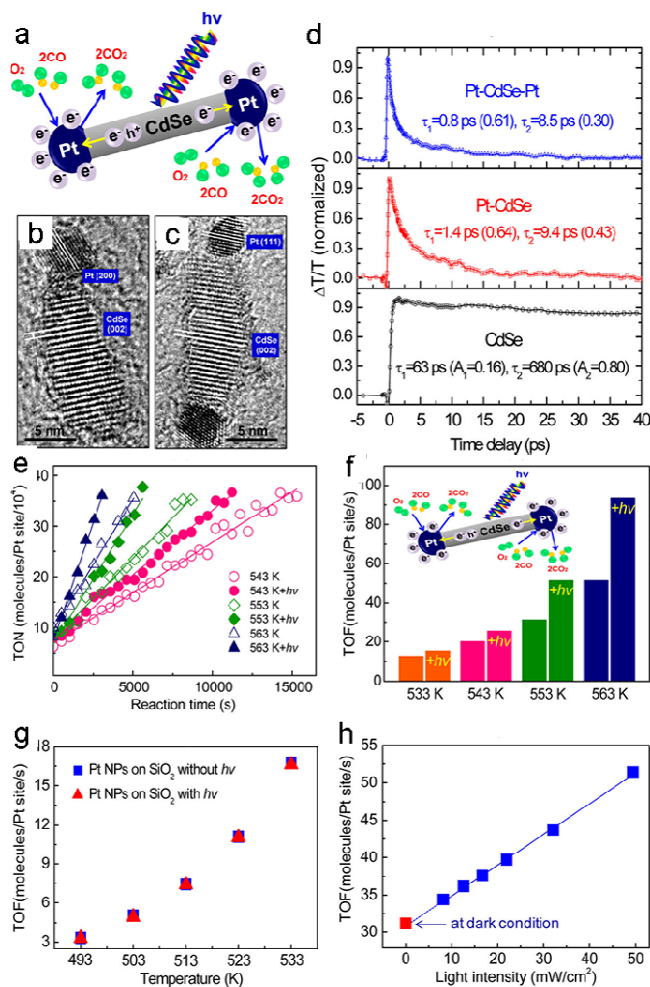


Fig. 13 (a) Scheme of hot-electron formation and catalysis in CO oxidation by O₂, TEM image of (b) singly and (c) doubly tipped Pt on CdSe nanorod, (d) pump-probe experiments of Pt-CdSe and CdSe, (e) Plots and (f) column graphs on the catalytic performance of Pt-CdSe at different temperatures, (g) data on catalysis of CO oxidation by Pt-SiO₂, (h) TOFs values under different intensities of illumination. Adapted with permission from ref. 128. Copyright 2013, American Chemical Society.

Furthermore, it is noted that, apart from the decoration of semiconductors with noble metals for nanocatalysis, some co-catalytic systems like CdS-MoS₂,¹³⁴ CdSe-MoS₂,¹³⁵ and other hybrid nanomaterials¹³⁶ have also received increasing interests,

especially in the area of photocatalysis. In such a context, very recently, our group has successfully synthesized 1D/2D helical CdS/ZnIn₂S₄ nano-heterostructures (Fig. 15). It was proposed that the mismatches in lattice and dangling bonds between 1D and 2D units are responsible for the formation of nano-heterostructures. The resultant well-defined interface between CdS nanowire and ZnIn₂S₄ nanosheet induces the delocalized interface states, thus facilitate the charge transfer and enhance the performance in the photoelectrochemical cells.¹³⁷ The results presented here are expected to open up exciting opportunities for the construction of more complex 1D/2D hybrid nanostructures with multifunctionalities. In view of the key role of noble metals in nanocatalysis, as a proof of concept, occasionally subsequent deposition of noble metals on these hybrid nanostructures could further enhance their catalytic performance.¹³⁸

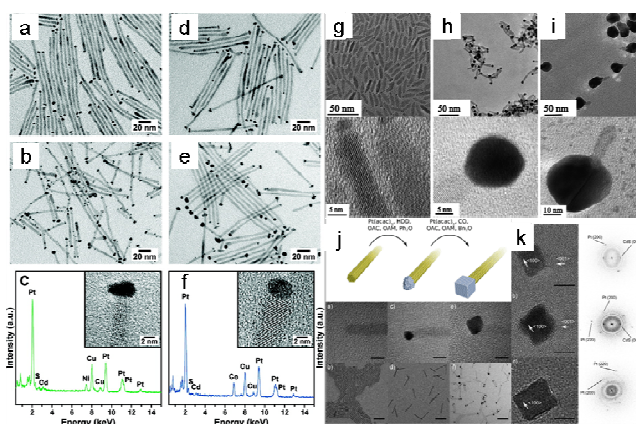


Fig. 14 (a-f) TEM and EDX analysis of the PtNi and PtCo on CdS nanorod, (g-i) growth of different-size gold tips on CdS nanorod, (j) growth of Pt nanocube on CdS nanorod, (k) HRTEM and SAED analysis on the crystal orientation. Adapted with permission from ref. 131. Copyright 2008, American Chemical Society. Adapted with permission from ref. 132. Copyright 2010, The Royal Society of Chemistry. Adapted with permission from ref. 133. Copyright 2013, WILEY-VCH Verlag GmbH & Co. KGaA, Weinheim.

2.4 Confined space nanointerfaces as nanoreactors

Finally, we would like to note some new type of nanointerface, especially the interface in the confined space. These confined spaces would introduce benefits such as enhanced stability or activity.

Metal on the inner wall of nanotubes

The first example involves the noble metal catalyst located in the inner surface of CNT. In CNTs, due to the rolling and

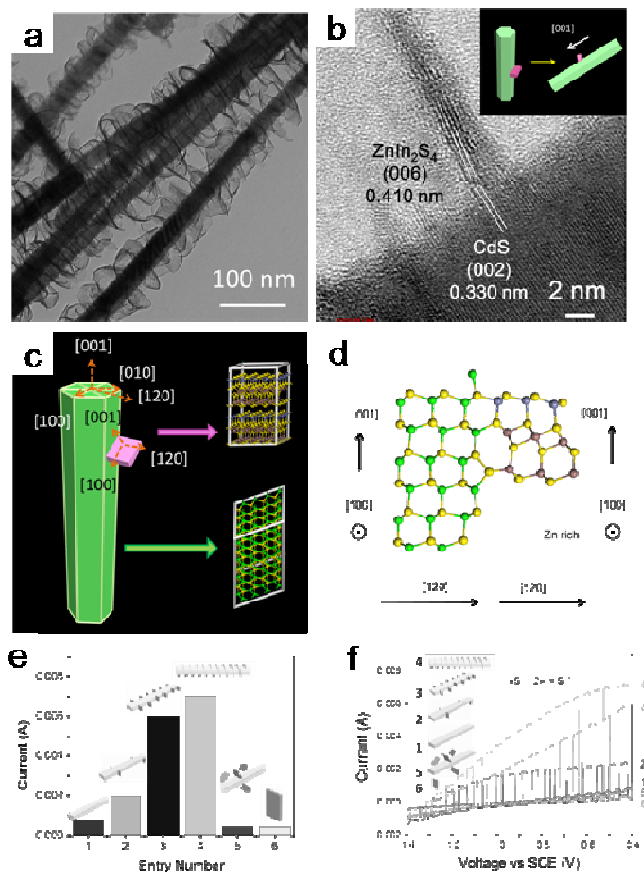


Fig. 15 (a) TEM, (b) HRTEM, (c) Model images of helical CdS nanowire/ZnIn₂S₄ nanosheet heterostructures. (d) The atom arrangement after DFT relaxation at the interface. Cd green, S yellow, Zn blue, In brown. (e) Comparison of photocurrents. (f) *i*-*V* scans of samples. Adapted with permission from ref. 137. Copyright 2014, WILEY-VCH Verlag GmbH & Co. KGaA, Weinheim.

corresponding stress, the pi-electron wave-function would differ between the inner and the outer wall of the CNT.¹³⁹ The incorporation of metal NPs inside this type of electron-conducting support would bring significantly different properties that do not only come from spatially confinement, as compared to conventional electron-insulating support, such as mesoporous silica. Based on this concept, Bao et al.¹⁴⁰ realized the site-selective deposition of the RhMn NPs through capillary forces of the tubes in a wet chemical approach (Fig. 16). The site-selective deposition of RhMn NPs inside the CNT leads to one order of magnitude of increase in reactivity for production of ethanol from CO and H₂. While the selectivity toward CH₄, a byproduct, also significantly decreased. The authors proposed that because the inner wall of the CNT was more electron-deficient, the dissociation of the C–O bond became easier, thus the overall TOF was increased. This brings light to new opportunities in the development of high-performance heterogeneous catalysts via confinement of metal NPs inside CNTs.^{141–143}

Besides CNT, inorganic nanotube could also be adopted to construct a nanointerface in confined space. Recently, Gong et al.¹⁴⁴ utilized Cu NP inside copper phyllosilicates (Cu₂Si₂O₅(OH)₂) nanotube (Fig. 17) as an efficient catalyst for the hydrogenation of dimethyl oxalate to produce ethanol. The selective loading of copper species inside or outside the nanotube was also controlled by capillaries. They have checked that the Cu NPs were efficiently loaded inside the tube by tilted-angle TEM. Similar to the case of CNT, this new type of nanoreactor showed enhanced reactivity and stability than Cu-outside-nanotube catalyst. They have discussed the possible reason for the enhancement might be the suitable [Cu(0)]/[Cu(0)+[Cu⁺]] ratio and the prolonged contact of the reactant gas with the copper NPs. The tunable length of the nanotube reactor would also influence the selectivity toward ethanol.

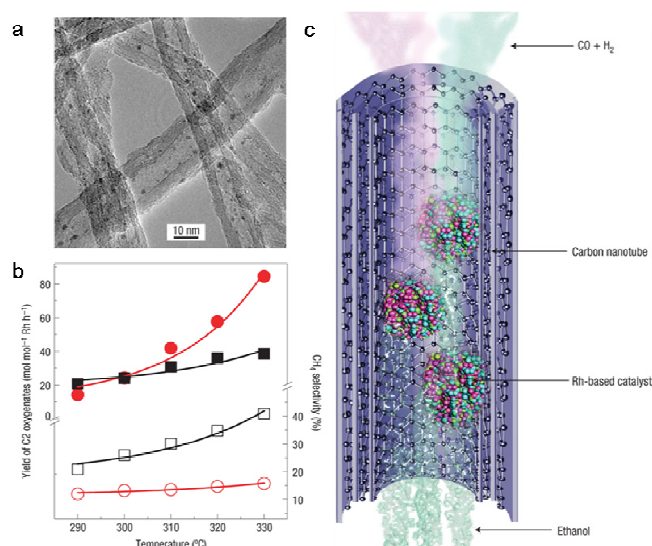


Fig. 16 (a) TEM image of Rh in CNT nanostructure, (b) yield of ethanol and selectivity of CH₄ at different temperatures for Rh in CNT and Rh on CNT structures, (c) schematic illustrations of the catalysis process inside a CNT. Adapted with permission from ref. 140. Copyright 2007, Nature Publishing Group.

Metal inside 3D porous support

During the last two decades, mesoporous materials were widely adopted as support materials in catalysis science.¹⁴⁵ The benefits from mesoporous support included higher thermal stability toward sintering, pore-size induced molecular selectivity and lower pack density, etc.¹⁴⁶ As this field has been intensively reviewed, we would not mention them. Recently, Metal organic frameworks (MOFs),¹⁴⁷ a new type of porous materials, have attracted tremendous attentions in the field of catalysis. Metal-inside-MOF materials are also intriguing and novel materials. By confining noble metal NCs inside MOF

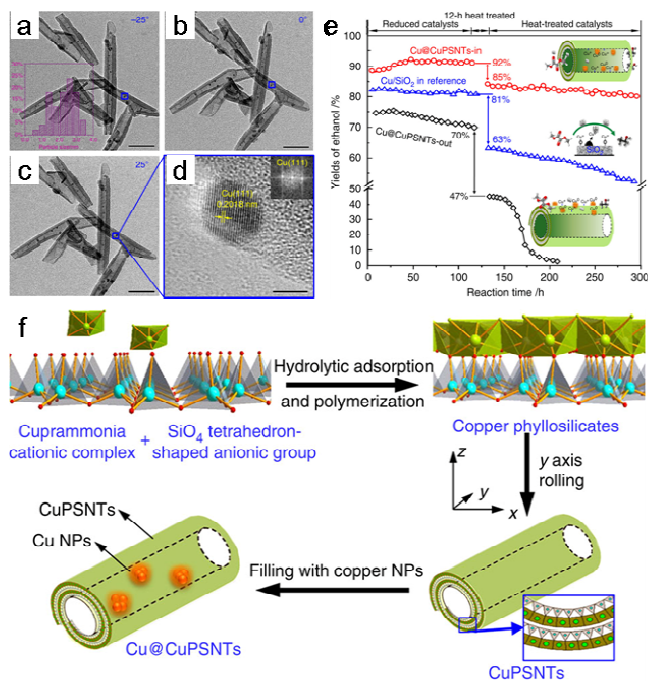


Fig. 17 (a-d) TEM at different tilted angles, (e) yield of ethanol at different reaction time, for different catalysts, (f) schemes on the formation process of Cu-in-CuPSNTs catalyst. Adapted with permission from ref. 144. Copyright 2013 Nature Publishing Group.

structures, these porous materials may serve as well-designed interface between reactants and the target catalysts, based on which the catalytic efficiency and selectivity of noble metal NCs may be enhanced. For example, Xu and co-workers¹⁴⁸ recently reported the use of “double solvents” approach to incorporate ultrafine Pt NPs into the cavities of MOFs (Pt@MIL-101), which show superior catalytic performance for solid-phase (ammonia borane thermal dehydrogenation), liquid-phase (ammonia borane hydrolysis), and gas-phase (CO oxidation) reactions. In fact, similar work has also been previously reported.¹⁴⁹⁻¹⁵¹ These results open up an opportunity to tune catalytic performance via the incorporation of ultrafine metal NPs (cluster) within highly porous MOFs. Another delicate example on fine tuning of metal-inside-MOF was presented recently by Huo et al.¹⁵² Through the addition of pre-synthesized PVP-capped NPs into synthetic solution of ZIF-8, various type of NPs, such as noble metal (Au, Pt), semiconductor (CdTe), Magnetic (Fe₃O₄), up conversion (NaYF₄:Yb) and polymer (polystyrene) were successfully encapsulated into well-controlled ZIF-8 NPs (Fig. 18). They proposed that PVP, as a polymer, played crucial role in this process as an efficient glue-like connector. The selective catalytic hydrogenation of alkenes with different molecular shapes by the Pt NPs and selective luminescent quenching of CdTe quantum dots were demonstrated. However, when using these types of materials in catalysis, high temperature should be avoided otherwise the organic part would be deteriorated.

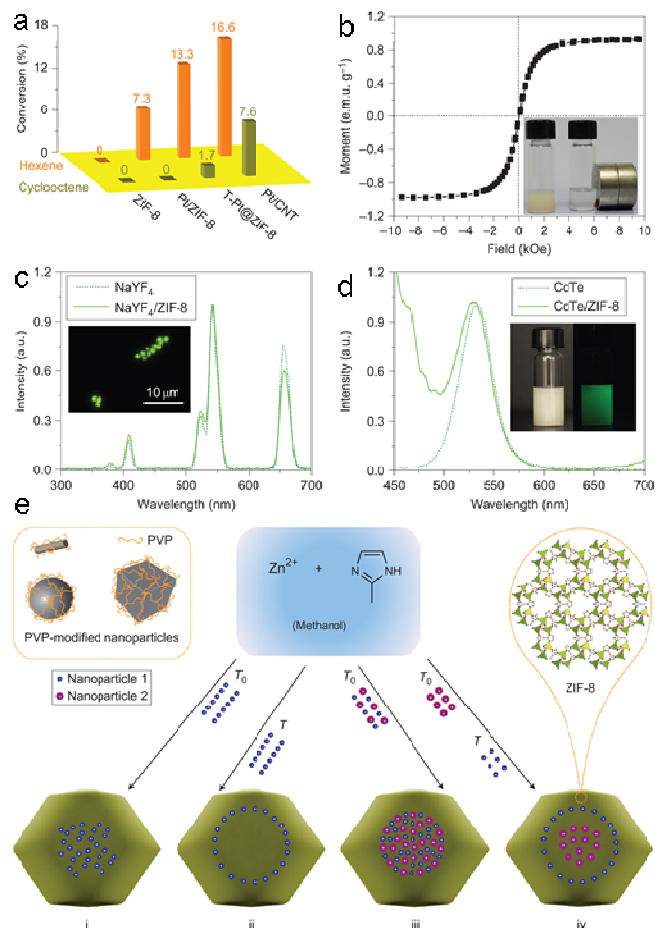


Fig. 18 (a) Catalytic conversion of hexene and cyclooctene for different catalysts, ZIF-8, Pt/ZIF-8, T-Pt@ZIF-8, Pt/CNT, (b) Magnetic property of Fe₃O₄@ZIF-8, (c) Up conversion spectra of NaYF₄@ZIF-8, (d) Fluorescence spectra of CdTe/ZIF-8, (e) Scheme on the incorporation of NPs into ZIF-8 NCs. Adapted with permission from ref. 152. Copyright 2012, Nature Publishing Group.

Very recently, our group has successfully prepared a series of well-defined MOF (MOF-5, Fe^{II}-MOF-5, Fe^{III}-MOF-5) and Fe^{III}-based infinite coordination polymer (ICP) hollow nanocages through one-pot solvothermal method. Impressively, by adding the pre-synthesized noble metal NPs into the synthetic solution of these hollow nanocages, the yolk-shell noble metal@MOF nanostructures can be fabricated. In the liquid-phase selective hydrogenation of 1-chloro-2-nitrobenzene, these yolk-shell structures show superior catalytic performance relative to the pure yolk (Fig. 19), which may arise from hydrogen enrichment in the MOF shells to accelerate the hydrogenation process, or the construction of hollow nanostructures serving as confined nanoreactors for catalysis.¹⁵³ Similar works for developing this concept have also been presently reported.¹⁵⁴⁻¹⁵⁶ Considering that MOF-based materials with tunable sizes and even chiral pore structures have been

well developed, great research potential can be expected in this field.

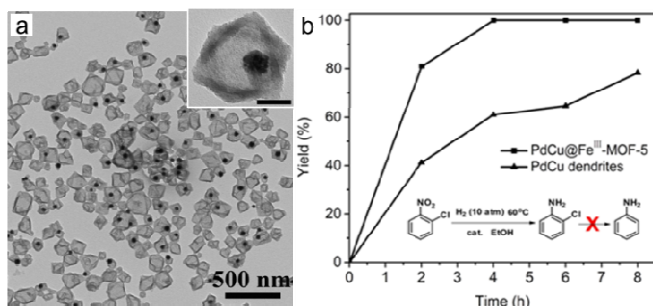


Fig. 19 (a) TEM images of the PdCu@Fe^{III}-MOF-5 yolk-shell structures produced by the encapsulation of pre-synthesized NPs in the Fe^{III}-MOF-5 hollow structures, (b) Yield (%) as a function of time in the selective hydrogenation of 1-chloro-2-nitrobenzene with PdCu dendrites and PdCu@Fe^{III}-MOF-5 yolk-shell structures. Adapted with permission from ref. 153. Copyright 2014, WILEY-VCH Verlag GmbH & Co. KGaA, Weinheim.

2.5 Methods for controlling well-defined interfaces

Rationally engineering interfaces to achieve high-performance catalysts has been demonstrated in various types of composite nanomaterials. To date, a wide variety of strategies have been developed towards the rational design and fine control of complex nanomaterials with well-defined interfaces. In the following, we focus our attention on the most commonly used and newly developed techniques of controlling well-defined interfaces, irrespective of the specific nanomaterial.

Direct deposition of pre-synthesized nanocrystals on supports with or without well-defined shapes

It's well known that heterogenous catalysts are complex systems, in which several parameters at least including particle size, structure, and composition of the supported NCs together with support usually strongly govern the performance of the catalysts. In most cases, it is inherently difficult to simultaneously optimize the catalysts by tuning these parameters for a desired reaction. Hence, to separate these complex factors in catalyst formulation and study them individually in a systematic manner, it is extremely meaningful to beforehand synthesize the single component with well-defined shapes. Then one can deposit the preformed NCs onto support to investigate interfacial effect in catalysis, in which the support with or without well-defined shapes can be used in view of specific purposes. If the deposition process does not change the sizes and shapes of supported NCs, then the effect of support on the catalytic activity can be indeed isolated from other factors, and vice versa. Currently, the colloidal deposition method has been applied to allow the deposition of metal on various

support nanomaterials involving the conductors, semiconductors, insulators, and so on.

Seed-based epitaxial growth

As a solution-phase analogue of conventional vapor-phase heteroepitaxial deposition, seed-based epitaxial growth has been commonly employed to fabricate composite nanomaterials with well-defined shapes, in which the seed serves as primary substrate center for accommodating secondary component. In most cases, core-shell and heterojunction nanostructures are often prepared by this approach. Uniform coverage of the secondary component on the preformed seed during the growth favors the formation of core-shell nanostructures, while the nucleation and growth of the epitaxial component on specific sites of the seed yields heterojunction or other hybrid nanostructures. What's more, the multi-shells on original seeds as a core can be fabricated by repeatedly using the seeded process, which can endow the nanomaterials with multifunctionality. In the seed-mediated growth process, the morphology of the final nanostructures is strongly guided by the structure, shape, and size of the seeds, and the seeded growth environment (e.g., reducing agent, solvent, capping agent, etc.). In the case of bimetallic NCs, it has been demonstrated that the interactions between the epitaxial domain and the preformed seed are highly dependent on several physical parameters such as lattice match, atomic radii, bond dissociation energies, correlation of surface and interfacial energies. In addition to the colloidal synthesis of bimetallic NCs, the epitaxial growth of noble metals on other substrates such as metal oxides/chalcogenides/carbides/nitrides has also been reported, which is generally driven by lattice match or interfacial energy between noble metal and substrate.

Shape-evolution of catalysts driven by lattice match or reactions

It is known that the nanometer-sized particles are usually thermally unstable relative to their bulk counterparts. In some cases, the changes in structure, size and surface composition of the NPs can be apparently observed during catalytic reaction in different reaction environments or at an elevated temperature,¹⁵⁷⁻¹⁶⁰ which may thus lead to the reconstruction of interface between two domains. In the case of the catalysis, these changes can endow the nanomaterials with distinctive reactivity. For example, Somorjai and co-workers¹⁵⁷ have demonstrated that the surface composition and chemical state of core-shell Rh_{0.5}Pd_{0.5} NPs can undergo dramatic and reversible changes in response to oxidizing or reducing condition. Recently, inspired from the Deacon catalyst in which RuO₂ can form epitaxial layers on the surfaces of Rutile TiO₂, our group recently investigated the shape evolution process of RuO₂ NPs on the surface of P25 TiO₂. It was found that size effects take place in this process and RuO₂ NPs with sizes ~sub-2nm can be transformed into epitaxial layers while NPs with larger sizes are not inclined to modulate their morphologies. Based on a thermodynamic model, we consider that the surface tension and

interfacial lattice match between the NPs and substrates could be responsible for such transformation process (Fig. 20).¹⁶¹ Recently, with the help of a DFT study, similar phenomena could have been found in other binary rutile MO_2 compounds ($M=\text{Ir, Ru, Sn, and Ti}$).¹⁶² Based on the above facts, careful characterizations and in-situ monitoring in the size, morphology, and surface/interface structure of the studied catalysts during the reaction are very important, which is suggestive for the fundamental understanding of interface effect in catalysis.

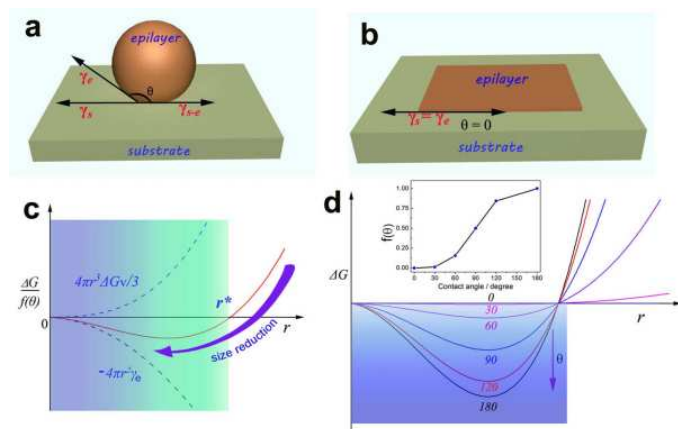


Fig. 20 Mechanism analysis of the stability of RuO_2 nanostructures on the surface of TiO_2 . (a) Interfacial tensions at the boundary between TiO_2 substrate and RuO_2 epitaxial nanoparticle with a large contact angle, modeling the surface structure of the initial catalyst prepared via hydrothermal method. (b) Surface structure of lattice-matched RuO_2 epilayer on the surface of TiO_2 , where the surface tension of the substrate (cs) is approximately equal to that of the epilayer (ce) because of the high degree of latticematch between RuO_2 and rutile. (c) Free energy diagram for the phase transition of a nanoparticle explaining the instability of sub-2-nm RuO_2 catalyst. (d) Effect of particle shape on the phase transition tendency of epitaxial layers on substrates expressed by the varied free energy change (ΔG). The inset is the diagram of angular factor $f(\theta)$, the function of contact angle that depicts the equilibrium particle shape on a substrate. Adapted with permission from ref. 161. Copyright 2012, Right Managed by Nature Publishing Group.

Polymer-assisted epitaxial growth as possible candidate

In comparison with conventional physical and chemical vapour-phase deposition techniques used for the epitaxial growth of noble metals or metal oxide on a bulk substrate, wet-chemical epitaxial growth has recently received considerable interests due to several advantages such as relatively low cost, ease of manipulation and versatility. As one of several chemical solution deposition approaches, polymer assisted epitaxial growth has attracted increasing attention and has been viewed as the most promising route, where metal ions are bound to polymers as the film precursor. At present, this route has been

extensively applied to produce high-quality films for a wide range of materials such as metal-oxides, metal-nitrides, metal-carbides, and single element.¹⁶³⁻¹⁶⁵ Moreover, the deposition of epitaxial phases can occur on exterior and interior surfaces of the substrates regardless of the sizes and shapes. The advantages of this technique lie in the homogeneous distribution of metal precursors in the solution and thus the ready formation of crack-free epitaxial films on the substrates in a conformal fashion. More importantly, to obtain improved functionalities, the composite nanomaterials can be coated on the surface of the substrates based on this method.

3 Conclusion and prospect

Nowdays, among various green chemistry and low environmental impact technologies towards renewable energy, catalysis has been regarded as the focus of such greener technologies, which in turn facilitates the production of nanomaterials, especially metal-based composite nanomaterials. Traditionally, it is difficult to gain a deep insight into the interfacial effect on catalytic performance in real working catalysts, arising from the coexistence of complex factors (shape, size, support effects, etc.). Thanks to the successful introduction of nanoscience to material synthesis, it now becomes possible to isolate the catalytic impact of each individual factor involved in the supported catalysts. Meanwhile, regarding design of novel and efficient catalysts towards renewable energy, it is crucial to maximize the interfacial area in a sense. Fundamental understanding of the interactions between two domains as well as their structural properties is essential for successful design and manipulation of complex nanomaterials with well-defined interfaces. The combination of different nanomaterials makes it possible to produce novel and/or enhanced functionalities that the individual component does not possess. To date, the wet-chemical synthesis has been recognized as one of the most promising strategies towards the fine control of complex nanomaterials with well-defined interfaces, involving metal-oxide, metal-metal, metal-non-oxide (e.g., chalcogenide, carbide, nitride, carbon, coordination polymer), and other interfaces. In the case of nanocatalysis, the prominent role of the interface between two components has been demonstrated by many experimental and theoretical investigations. Having said that, much more research efforts still have to be dedicated to unveil the intrinsic catalytic mechanism involved in complex reactions.

In the literatures, it has been established that the interactions between metal and attached domain generally arise from several factors such as electronic, steric, lattice strain or ensemble effects. However, in spite of previous research efforts, the amphibolic or inconclusive reaction mechanism over the studied catalysts is still usually proposed, resulting from inadequate nanomaterials characterization and the interference of numerous complicated factors such as organic capping agent, structure change, reaction condition, and so on. In particular, it should be mentioned that in most cases the

capping ligands are often used to direct the synthesis of uniform nanomaterials, which may hinder the catalytic activity to some extent. Therefore, developing surfactant-free synthesis or surface-clean strategies to design high-performance catalysts is especially required and deserves more studies. Furthermore, to meet the versatile demand in the catalysis, the accurate construction of complex nanomaterials with multiple synergic functions remains a major challenge and still need to be extensively explored, which requires developing a higher degree of synthetic ingenuity and creativity.

Acknowledgements

This work was supported by NSFC (91127040, 21221062), CPSF (2013M540085), and the State Key Project of Fundamental Research for Nanoscience and Nanotechnology (2011CB932402).

Notes and references

- M. Stratakis and H. Garcia, *Chem. Rev.*, 2012, **112**, 4469–4506.
- Y. Yin and A. P. Alivisatos, *Nature*, 2005, **437**, 664–670.
- J. M. De Teresa, A. Barthélémy, A. Fert, J. P. Contour, F. Montaigne and P. Seneor, *Science*, 1999, **286**, 507–509.
- T. Akita, M. Kohyama and M. Haruta, *Acc. Chem. Res.*, 2013, **46**, 1773–1782.
- M. Cargnello, J. J. D. Jaén, J. C. H. Garrido, K. Bakhtmutsky, T. Montini, J. J. C. Gámez, R. J. Gorte and P. Fornasiero, *Science*, 2012, **337**, 713–717.
- I. X. Green, W. Tang, M. Neurock and J. T. Yates, *Science*, 2011, **333**, 736–739.
- C. K. Costello, M. C. Kung, H. S. Oh, Y. Wang and H. H. Kung, *App. Cata. A: Gen.*, 2002, **232**, 159–168.
- H. H. Kung, M. C. Kung and C. K. Costello, *J. Cata.*, 2003, 216, 425–432.
- M. Haruta, *Faraday Discuss.*, 2011, **152**, 11–32.
- Y. Y. Wu, N. A. Mashayekhi and H. H. Kung, *Cata. Sci. & Tech.*, 2013, **3**, 2881–2891.
- M. M. Schubert, S. Hackenberg, A. C. van Veen, M. Muhler, V. Plzak and R. J. Behm, *J. Cata.*, 2001, **197**, 113–122.
- Q. Fu and T. Wagner, *Surf. Sci. Rep.*, 2007, **62**, 431–498.
- J. Gong, Z. Nie and X. Ma, *Phys. Chem. Chem. Phys.*, 2013, **15**, 11985–11987.
- A. Chen and P. Holt-Hindle, *Chem. Rev.*, 2010, **110**, 3767–3804.
- A. T. Bell, *Science*, 2003, **299**, 1688–1691.
- N. Mizuno and M. Misono, *Chem. Rev.*, 1998, **98**, 199–218.
- G. C. Bond, *Heterogeneous catalysis*, 1987.
- C. N. Satterfield, *Heterogeneous catalysis in industrial practice*. 2nd edition, 1991.
- S. J. Tauster, S. C. Fung and R. L. Garten, *J. Am. Chem. Soc.*, 1978, **100**, 170–175.
- D. W. Goodman, *Catal. Lett.*, 2005, **99**, 1–4.
- D. Matthey, J. G. Wang, S. Wendt, J. Matthiesen, R. Schaub, E. Lægsgaard, B. Hammer and F. Besenbacher, *Science*, 2007, **315**, 1692–1696.
- I. X. Green, W. Tang, M. Neurock and J. T. Yates, *Angew. Chem. Int. Ed.*, 2011, **50**, 10186–10189.
- K. Mudiyansele, S. D. Senanayake, L. Feria, S. Kundu, A. E. Baber, J. Graciani, A. B. Vidal, S. Agnoli, J. Evans, R. Chang, S. Axnanda, Z. Liu, J. F. Sanz, P. Liu, J. A. Rodriguez and D. J. Stacchiola, *Angew. Chem. Int. Ed.*, 2013, **52**, 5101–5105.
- N. López and F. Illas, *J. Phys. Chem. B*, 1998, **102**, 1430–1436.
- X. Nie, H. Qian, Q. Ge, H. Xu and R. Jin, *ACS Nano*, 2012, **6**, 6014–6022.
- J. Lin, A. Wang, B. Qiao, X. Liu, X. Yang, X. Wang, J. Liang, J. Li, J. Liu and T. Zhang, *J. Am. Chem. Soc.*, 2013, **135**, 15314–15317.
- B. Qiao, A. Wang, X. Yang, L. F. Allard, Z. Jiang, Y. Cui, J. Liu, J. Li and T. Zhang, *Nat. Chem.*, 2011, **3**, 634–641.
- Z.-C. Zhang, X. Zhang, Q.-Y. Yu, Z.-C. Liu, C.-M. Xu, J.-S. Gao, J. Zhuang and X. Wang, *Chem. A Eur. J.*, 2012, **18**, 2639–2645.
- T. Fujita, P. Guan, K. McKenna, X. Lang, A. Hirata, L. Zhang, T. Tokunaga, S. Arai, Y. Yamamoto, N. Tanaka, Y. Ishikawa, N. Asao, Y. Yamamoto, J. Erlebacher and M. Chen, *Nat. Mater.*, 2012, **11**, 775–780.
- X. Zhang, H. Wang and B.-Q. Xu, *J. Phys. Chem. B*, 2005, **109**, 9678–9683.
- S. Panigrahi, S. Basu, S. Praharaj, S. Pande, S. Jana, A. Pal, S. K. Ghosh and T. Pal, *J. Phys. Chem. C*, 2007, **111**, 4596–4605.
- H. Lee, S. E. Habas, S. Kweskin, D. Butcher, G. A. Somorjai and P. Yang, *Angew. Chem. Int. Ed.*, 2006, **45**, 7824–7828.
- N. Zheng and G. D. Stucky, *J. Am. Chem. Soc.*, 2006, **128**, 14278–14280.
- M. Comotti, W.-C. Li, B. Spliethoff and F. Schüth, *J. Am. Chem. Soc.*, 2005, **128**, 917–924.
- M. Cargnello, V. V. T. Doan-Nguyen, T. R. Gordon, R. E. Diaz, E. A. Stach, R. J. Gorte, P. Fornasiero and C. B. Murray, *Science*, 2013, **341**, 771–773.
- J. Zhang, H. Yang, J. Fang and S. Zou, *Nano Lett.*, 2010, **10**, 638–644.
- J. Wu, J. Zhang, Z. Peng, S. Yang, F. T. Wagner and H. Yang, *J. Am. Chem. Soc.*, 2010, **132**, 4984–4985.
- H. Zhang, M. Jin, H. Liu, J. Wang, M. J. Kim, D. Yang, Z. Xie, J. Liu and Y. Xia, *ACS Nano*, 2011, **5**, 8212–8222.
- G. Chen, H. Yang, B. Wu, Y. Zheng and N. Zheng, *Dalton Trans.*, 2013, **42**, 12699–12705.
- E. Higuchi, A. Taguchi, K. Hayashi and H. Inoue, *J. Electro. Chem.*, 2011, **663**, 84–89.
- E. Higuchi, K. Adachi, S. Nohara and H. Inoue, *Res. Chem. Intermed.*, 2009, **35**, 985–995.
- F. Lin, D. Hoang, C.-K. Tsung, W. Huang, S.-Y. Lo, J. Wood, H. Wang, J. Tang and P. Yang, *Nano Res.*, 2011, **4**, 61–71.
- F. L. Liao, Y. Q. Huang, J. W. Ge, W. R. Zheng, K. Tedsree, P. Collier, X. L. Hong, S. C. Tsang, *Angew. Chem. Int. Ed.*, 2011, **50**, 2162–2165.
- X. W. Zhou, J. Qu, F. Xu, J. P. Hu, J. S. Foord, Z. Y. Zeng, X. L. Hong, S. C. E. Tsang, *Chem. Commun.*, 2013, **49**, 1747–1749.
- L. Li, X. Chen, Y. Wu, D. Wang, Q. Peng, G. Zhou and Y. Li, *Angew. Chem. Int. Ed.*, 2013, **52**, 11049–11053.
- H. Yu, M. Chen, P. M. Rice, S. X. Wang, R. L. White and S. Sun, *Nano Lett.*, 2005, **5**, 379–382.

47. H. Yin, C. Wang, H. Zhu, S. H. Overbury, S. Sun and S. Dai, *Chem. Commun.*, 2008, 4357–4359.
48. C. Wang, H. Yin, S. Dai and S. Sun, *Chem. Mater.*, 2010, **22**, 3277–3282.
49. Y. Lee, A. Loew and S. Sun, *Chem. Mater.*, 2009, **22**, 755–761.
50. C. Xu, B. Wang and S. Sun, *J. Am. Chem. Soc.*, 2009, **131**, 4216–4217.
51. B. Wu, H. Zhang, C. Chen, S. Lin and N. Zheng, *Nano Res.*, 2009, **2**, 975–983.
52. Y. Zhai, L. Jin, P. Wang and S. Dong, *Chem. Commun.*, 2011, **47**, 8268–8270.
53. C. Wang, H. Daimon and S. Sun, *Nano Lett.*, 2009, **9**, 1493–1496.
54. M. J. Bradley, A. J. Biacchi and R. E. Schaak, *Chem. Mater.*, 2013, **25**, 1886–1892.
55. X. Sun, S. Guo, Y. Liu and S. Sun, *Nano Lett.*, 2012, **12**, 4859–4863.
56. A. Figuerola, A. Fiore, R. Di Corato, A. Falqui, C. Giannini, E. Micotti, A. Lascialfari, M. Corti, R. Cingolani, T. Pellegrino, P. D. Cozzoli and L. Manna, *J. Am. Chem. Soc.*, 2008, **130**, 1477–1487.
57. H. Gu, Z. Yang, J. Gao, C. K. Chang and B. Xu, *J. Am. Chem. Soc.*, 2004, **127**, 34–35.
58. Y. Pan, J. Gao, B. Zhang, X. Zhang and B. Xu, *Langmuir*, 2009, **26**, 4184–4187.
59. S.-H. Choi, H. B. Na, Y. I. Park, K. An, S. G. Kwon, Y. Jang, M.-h. Park, J. Moon, J. S. Son, I. C. Song, W. K. Moon and T. Hyeon, *J. Am. Chem. Soc.*, 2008, **130**, 15573–15580.
60. M. Casavola, V. Grillo, E. Carlino, C. Giannini, F. Gozzo, E. Fernandez Pinel, M. A. Garcia, L. Manna, R. Cingolani and P. D. Cozzoli, *Nano Lett.*, 2007, **7**, 1386–1395.
61. C. George, A. Genovese, A. Casu, M. Prato, M. Povia, L. Manna and T. Montanari, *Nano Lett.*, 2013, **13**, 752–757.
62. Y. Yamada, C.-K. Tsung, W. Huang, Z. Huo, S. E. Habas, T. Soejima, C. E. Aliaga, G. A. Somorjai and P. Yang, *Nat. Chem.*, 2011, **3**, 372–376.
63. A. Horváth, A. Beck, A. Sárkány, G. Stefler, Z. Varga, O. Geszti, L. Tóth and L. Gucci, *J. Phys. Chem. B*, 2006, **110**, 15417–15425.
64. Z. Ma, S. Brown, J. Y. Howe, S. H. Overbury and S. Dai, *J. Phys. Chem. C*, 2008, **112**, 9448–9457.
65. H. Yin, Z. Ma, S. H. Overbury and S. Dai, *J. Phys. Chem. C*, 2008, **112**, 8349–8358.
66. P. Lu, C. T. Campbell and Y. Xia, *Nano Lett.*, 2013, **13**, 4957–4962.
67. A. Horváth, A. Beck, G. Stefler, T. Benkó, G. Sáfrán, Z. Varga, J. Gubicza and L. Gucci, *J. Phys. Chem. C*, 2011, **115**, 20388–20398.
68. Q. Fu, F. Yang and X. Bao, *Acc. Chem. Res.*, 2013, **46**, 1692–1701.
69. X. Wang, H. Yu, D. Hua and S. Zhou, *J. Phys. Chem. C*, 2013, **117**, 7294–7302.
70. L. Chen, C. K. S. Choong, Z. Zhong, L. Huang, T. P. Ang, L. Hong and J. Lin, *J. Catal.*, 2010, **276**, 197–200.
71. R. Mu, Q. Fu, H. Xu, H. Zhang, Y. Huang, Z. Jiang, S. Zhang, D. Tan and X. Bao, *J. Am. Chem. Soc.*, 2011, **133**, 1978–1986.
72. J. A. Rodriguez, J. Graciani, J. Evans, J. B. Park, F. Yang, D. Stacchiola, S. D. Senanayake, S. Ma, M. Pérez, P. Liu, J. F. Sanz and J. Hrbek, *Angew. Chem. Int. Ed.*, 2009, **48**, 8047–8050.
73. D. Wang and Y. Li, *Adv. Mater.*, 2011, **23**, 1044–1060.
74. R. Ferrando, J. Jellinek and R. L. Johnston, *Chem. Rev.*, 2008, **108**, 845–910.
75. D. Wang, Q. Peng and Y. Li, *Nano Res.*, 2010, **3**, 574–580.
76. B. Wu and N. Zheng, *Nano Today*, 2013, **8**, 168–197.
77. Q. Yuan, Z. Zhou, J. Zhuang and X. Wang, *Chem. Commun.*, 2010, **46**, 1491–1493.
78. Z.-C. Zhang, J.-F. Hui, Z.-G. Guo, Q.-Y. Yu, B. Xu, X. Zhang, Z.-C. Liu, C.-M. Xu, J.-S. Gao and X. Wang, *Nanoscale*, 2012, **4**, 2633–2639.
79. Z. Zhang, Y. Yang, F. Nosheen, P. Wang, J. Zhang, J. Zhuang and X. Wang, *Small*, 2013, **9**, 3063–3069.
80. Q. Yuan, Z. Zhou, J. Zhuang and X. Wang, *Chem. Mater.*, 2010, **22**, 2395–2402.
81. F. Nosheen, Z.-c. Zhang, J. Zhuang and X. Wang, *Nanoscale*, 2013, **5**, 3660–3663.
82. Q. Yuan and X. Wang, *Nanoscale*, 2010, **2**, 2328–2335.
83. F. J. Vidal-Iglesias, A. Lopez-Cudero, J. Solla-Gullon, J. M. Feliu, *Angew. Chem. Int. Ed.*, 2013, **52**, 964–967.
84. R. G. Chaudhuri, S. Paria, *Chem. Rev.*, 2012, **112**, 2373–2433.
85. S. E. Habas, H. Lee, V. Radmilovic, G. A. Somorjai and P. Yang, *Nat. Mater.*, 2007, **6**, 692–697.
86. D. Kim, Y. W. Lee, S. B. Lee and S. W. Han, *Angew. Chem. Int. Ed.*, 2012, **51**, 159–163.
87. C.-L. Lu, K. S. Prasad, H.-L. Wu, J.-a. A. Ho and M. H. Huang, *J. Am. Chem. Soc.*, 2010, **132**, 14546–14553.
88. F.-R. Fan, D.-Y. Liu, Y.-F. Wu, S. Duan, Z.-X. Xie, Z.-Y. Jiang and Z.-Q. Tian, *J. Am. Chem. Soc.*, 2008, **130**, 6949–6951.
89. S. Guo, S. Zhang, D. Su and S. Sun, *J. Am. Chem. Soc.*, 2013, **135**, 13879–13884.
90. B. T. Sneed, C. N. Brodsky, C.-H. Kuo, L. K. Lamontagne, Y. Jiang, Y. Wang, F. Tao, W. Huang and C.-K. Tsung, *J. Am. Chem. Soc.*, 2013, **135**, 14691–14700.
91. Y. Wu, D. Wang, X. Chen, G. Zhou, R. Yu and Y. Li, *J. Am. Chem. Soc.*, 2013, **135**, 12220–12223.
92. H. Yang, *Angew. Chem. Int. Ed.*, 2011, **50**, 2674–2676.
93. G.-R. Zhang, D. Zhao, Y.-Y. Feng, B. Zhang, D. S. Su, G. Liu and B.-Q. Xu, *ACS Nano*, 2012, **6**, 2226–2236.
94. B. Lim, M. Jiang, P. H. C. Camargo, E. C. Cho, J. Tao, X. Lu, Y. Zhu and Y. Xia, *Science*, 2009, **324**, 1302–1305.
95. Y. Feng, J. He, H. Wang, Y. Y. Tay, H. Sun, L. Zhu and H. Chen, *J. Am. Chem. Soc.*, 2012, **134**, 2004–2007.
96. J.-s. Choi, Y.-w. Jun, S.-I. Yeon, H. C. Kim, J.-S. Shin and J. Cheon, *J. Am. Chem. Soc.*, 2006, **128**, 15982–15983.
97. B. Lim, H. Kobayashi, T. Yu, J. Wang, M. J. Kim, Z.-Y. Li, M. Rycenga and Y. Xia, *J. Am. Chem. Soc.*, 2010, **132**, 2506–2507.
98. P. H. C. Camargo, Y. Xiong, L. Ji, J. M. Zuo and Y. Xia, *J. Am. Chem. Soc.*, 2007, **129**, 15452–15453.
99. T. P. Vinod, M. Yang, J. Kim and N. A. Kotov, *Langmuir*, 2009, **25**, 13545–13550.
100. X. Huang and N. Zheng, *J. Am. Chem. Soc.*, 2009, **131**, 4602–4603.
101. D. Wang and Y. Li, *J. Am. Chem. Soc.*, 2010, **132**, 6280–6281.
102. L. Wang, Y. Nemoto and Y. Yamauchi, *J. Am. Chem. Soc.*, 2011, **133**, 9674–9677.
103. C.-H. Cui, J.-W. Yu, H.-H. Li, M.-R. Gao, H.-W. Liang and S.-H. Yu, *ACS Nano*, 2011, **5**, 4211–4218.
104. C.-H. Cui and S.-H. Yu, *Acc. Chem. Res.*, 2013, **46**, 1427–1437.
105. H. Dai, *Acc. Chem. Res.*, 2002, **35**, 1035–1044.
106. A. K. Geim and K. S. Novoselov, *Nat. Mater.*, 2007, **6**, 183–191.

- 107.Y. Wang, X. Wang and M. Antonietti, *Angew. Chem. Int. Ed.*, 2012, **51**, 68–89.
- 108.G. G. Wildgoose, C. E. Banks and R. G. Compton, *Small*, 2006, **2**, 182–193.
- 109.B. F. Machado and P. Serp, *Cata. Sci. & Tech.*, 2012, **2**, 54–75.
- 110.M. Yang, Z. Cui and F. J. DiSalvo, *Phys. Chem. Chem. Phys.*, 2013, **15**, 1088–1092.
- 111.Z. Qiu, H. Huang, J. Du, T. Feng, W. Zhang, Y. Gan and X. Tao, *J. Phys. Chem. C*, 2013, **117**, 13770–13775.
- 112.D. Wang and Y. Li, *Chem. Commun.*, 2011, **47**, 3604–3606.
- 113.L. De Trizio, F. De Donato, A. Casu, A. Genovese, A. Falqui, M. Povia and L. Manna, *ACS Nano*, 2013, **7**, 3997–4005.
- 114.Y. J. Tong, *Chem. Soc. Rev.*, 2012, **41**, 8195–8209.
- 115.F. E. Osterloh, *Chem. Mater.*, 2007, **20**, 35–54.
- 116.J. F. Reber and M. Rusek, *J. Phys. Chem.*, 1986, **90**, 824–834.
- 117.J. Yang, D. Wang, H. Han and C. Li, *Acc. Chem. Res.*, 2013, **46**, 1900–1909.
- 118.G. Dukovic, M. G. Merkle, J. H. Nelson, S. M. Hughes and A. P. Alivisatos, *Adv. Mater.*, 2008, **20**, 4306–4311.
- 119.E. Elmalem, A. E. Saunders, R. Costi, A. Salant and U. Banin, *Adv. Mater.*, 2008, **20**, 4312–4317.
- 120.A. Vaneski, A. S. Susha, J. Rodriguez-Fernandez, M. Berr, F. Jackel, J. Feldmann and A. L. Rogach, *Adv. Mater.*, 2011, **21**, 1547–1556.
- 121.L. Amirav and A. P. Alivisatos, *J. Phys. Chem. Lett.*, 2010, **1**, 1051–1054.
- 122.E. Khon, K. Lambright, R. S. Khnayzer, P. Moroz, D. Perera, E. Butaeva, S. Lambright, F. N. Castellano and M. Zamkov, *Nano Lett.*, 2013, **13**, 2016–2023.
- 123.M. Berr, A. Vaneski, A. S. Susha, J. Rodriguez-Fernandez, M. Doblinger, F. Jackel, A. L. Rogach and J. Feldmann, *Appl. Phys. Lett.*, 2010, **97**, 093108.
- 124.J. Yang and J. Y. Ying, *Angew. Chem. Int. Ed.*, 2011, **50**, 4637–4643.
- 125.T. F. Jaramillo, K. P. Jørgensen, J. Bonde, J. H. Nielsen, S. Horch and I. Chorkendorff, *Science*, 2007, **317**, 100–102.
- 126.X. Huang, Z. Zeng, S. Bao, M. Wang, X. Qi, Z. Fan and H. Zhang, *Nat. Commun.*, 2013, **4**, 1444.
- 127.R. T. Ross and A. J. Nozik, *J. App. Phys.*, 1982, **53**, 3813–3818.
- 128.S. M. Kim, S. J. Lee, S. H. Kim, S. Kwon, K. J. Yee, H. Song, G. A. Somorjai and J. Y. Park, *Nano Lett.*, 2013, **13**, 1352–1358.
- 129.Y. Li, E. Boone and M. A. El-Sayed, *Langmuir*, 2002, **18**, 4921–4925.
- 130.D. Xu, Z. Liu, H. Yang, Q. Liu, J. Zhang, J. Fang, S. Zou and K. Sun, *Angew. Chem. Int. Ed.*, 2009, **48**, 4217–4221.
- 131.S. E. Habas, P. Yang and T. Mokari, *J. Am. Chem. Soc.*, 2008, **130**, 3294–3295.
- 132.C. O'Sullivan, R. D. Gunning, C. A. Barrett, A. Singh and K. M. Ryan, *J. Mater. Chem.*, 2010, **20**, 7875–7880.
- 133.H. Schlicke, D. Ghosh, L.-K. Fong, H. L. Xin, H. Zheng and A. P. Alivisatos, *Angew. Chem. Int. Ed.*, 2013, **52**, 980–982.
- 134.X. Zong, H. Yan, G. P. Wu, G. J. Ma, F. Y. Wen, L. Wang and C. Li, *J. Am. Chem. Soc.*, 2008, **130**, 7176–7177.
- 135.F. A. Frame and F. E. Osterloh, *J. Phys. Chem. C*, 2010, **114**, 10628–10633.
- 136.K. Maeda and K. Domen, *J. Phys. Chem. Lett.*, 2010, **1**, 2655–2661.
- 137.B. Xu, P. L. He, H. L. Liu, P. P. Wang, G. Zhou and X. Wang, *Angew. Chem. Int. Ed.*, 2014, **53**, 2339–2343.
- 138.X. W. Wang, G. Liu, L. Z. Wang, Z. G. Chen, G. Q. Lu and H. M. Cheng, *Adv. Energy. Mater.*, 2012, **2**, 42–46.
- 139.X. Blase, L. X. Benedict, E. L. Shirley and S. G. Louie, *Phys. Rev. Lett.*, 1994, **72**, 1878–1881.
- 140.X. Pan, Z. Fan, W. Chen, Y. Ding, H. Luo and X. Bao, *Nat. Mater.*, 2007, **6**, 507–511.
- 141.X. Pan and X. Bao, *Chem. Commun.*, 2008, 6271–6281.
- 142.X. Pan and X. Bao, *Acc. Chem. Res.*, 2011, **44**, 553–562.
- 143.X. Zhang, Y. C. Guo, Z. C. Zhang, J. S. Gao and C. M. Xu, *J. Catal.*, 2012, **292**, 213–226.
- 144.H. Yue, Y. Zhao, S. Zhao, B. Wang, X. Ma and J. Gong, *Nat. Commun.*, 2013, **4**, 2339–2346.
- 145.A. Corma, *Chem. Rev.*, 1997, **97**, 2373–2420.
- 146.W. Li, Q. Yue, Y. Deng and D. Zhao, *Adv. Mater.*, 2013, **25**, 5128–5128.
- 147.H.-C. Zhou, J. R. Long and O. M. Yaghi, *Chem. Rev.*, 2012, **112**, 673–674.
- 148.A. Aijaz, A. Karkamkar, Y. J. Choi, N. Tsumori, E. Ronnebro, T. Autrey, H. Shioyama and Q. Xu, *J. Am. Chem. Soc.*, 2012, **134**, 13926–13929.
- 149.M. S. El-Shall, V. Abdelsayed, A. E. R. S. Khder, H. M. A. Hassan, H. M. El-Kaderi and T. E. Reich, *J. Mater. Chem.*, 2009, **19**, 7625–7631.
- 150.C. Wang, K. E. deKrafft and W. B. Lin, *J. Am. Chem. Soc.*, 2012, **134**, 7211–7214.
- 151.F. Schroder, D. Esken, M. Cokoja, M. W. E. Van den Berg, O. I. Lebedev, G. V. Tendeloo, B. Walaszek, G. Buntkowsky, H.-H. Limbach, B. Chaudret and R. A. Fischer, *J. Am. Chem. Soc.*, 2008, **130**, 6119–6130.
- 152.G. Lu, S. Li, Z. Guo, O. K. Farha, B. G. Hauser, X. Qi, Y. Wang, X. Wang, S. Han, X. Liu, J. S. DuChene, H. Zhang, Q. Zhang, X. Chen, J. Ma, S. C. J. Loo, W. D. Wei, Y. Yang, J. T. Hupp and F. Huo, *Nat. Chem.*, 2012, **4**, 310–316.
- 153.Z. -C, Zhang, Y. -F. Chen, X. -B, Xu, J. -C, Zhang, G. -L. Xiang, W. He, X. Wang, *Angew. Chem. Int. Ed.*, 2014, **53**, 429–433.
- 154.M. T. Zhao, K. Deng, L. C. He, Y. Liu, G. D. Li, H. J. Zhao, Z. Y. Tang, *J. Am. Chem. Soc.*, 2014, **136**, 1738–1741.
- 155.Y. Y. Liu, W. N. Zhang, S. Z. Li, C. L. Cui, J. Wu, H. Y. Chen and F. W. Huo, *Chem. Mater.*, 2014, **26**, 1119–1125.
- 156.L. C. He, Y. Liu, J. Z. Liu, Y. S. Xiong, J. Z. Zheng, Y. L. Liu and Z. Y. Tang, *Angew. Chem. Int. Ed.*, 2013, **52**, 3741–3745.
- 157.F. Tao, M. E. Grass, Y. -W. Zhang, D. R. Butcher, J. R. Renzas, Z. Liu, J. Y. Chung, B. S. Mun, M. Salmeron, G. A. Somorjai, *Science*, 2008, **322**, 932–934.
- 158.F. Tao, Sefa Dag, L. -W. Wang, Z. Liu, D. R. Butcher, H. Bluhm, M. Salmeron, G. A. Somorjai, *Science*, 2010, **327**, 850–853.
- 159.J. A. Rodriguez, D. W. Goodman, *Science*, 2007, **257**, 897–903.
- 160.S. Hu, X. Wang, *Chem. Soc. Rev.*, 2013, **42**, 5577–5594.
- 161.G. -L, Xiang, X. -J, Shi, Y. -L, Wu, J. Zhuang, X. Wang, *Sci. Rep.*, 2012, **2**, 801–806.
- 162.G. Novell-Leruth, G. Carchini, N. Lopez, *J. Chem. Phys.*, 2013, **138**, 194706–194716.
- 163.G. -F, Zou, J. Zhao, H. -M, Luo, T. M. McCleskey, A. K. Burrell, Q. -X, Jia, *Chem. Soc. Rev.*, 2013, **42**, 439–449.

- 164.Q. -X. Jia, T. M. McCleskey, A. K. Burrell, Y. Lin, G. E. Collis, H. Wang, A. D. Q. Li, *Nat. Mater.*, 2004, **3**, 529–532.
- 165.A. K. Burrell, T. M. McCleskey, Q. X. Jia, *Chem. Commun.*, 2008, 1271–1277.



Zhicheng Zhang is currently a postdoc researcher in Professor Xun Wang's group in Department of Chemistry from Tsinghua University, China. He received his bachelor's degree in College of Chemistry and Chemical Engineering from Southwest Petroleum University, China (2007), and his PhD degree from College of Chemical Engineering, China University of Petroleum, Beijing, China (2012). His current research interests include synthesis, characterization and applications of noble metal-based nanocrystals.



Biao Xu is currently a PhD candidate in Professor Xun Wang's group. He received his BS degree in chemistry from Tsinghua University in 2009. His research interests include synthesis, properties and applications of water-soluble compound semiconductor nanocrystals.



Professor Xun Wang received his PhD degree from the Department of Chemistry, Tsinghua University in 2004. He then joined the faculty of the Department of Chemistry, Tsinghua University in 2004, and was promoted to associate professor and full professor in 2005 and 2007, respectively. His current research interests include synthetic methodology, formation mechanism, and properties of monodisperse nanocrystals.

